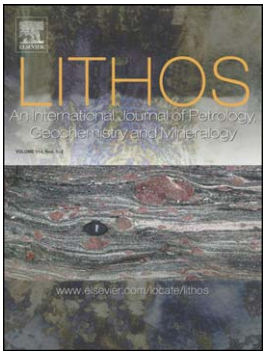

Geochronology, geochemistry and Nd, Sr and Pb isotopes of syn-orogenic granodiorites and granites (Damara orogen, Namibia) – arc-related plutonism or melting of mafic crustal sources?

L. Osterhus, S. Jung, J. Berndt, F. Hauff

PII: S0024-4937(14)00155-8
DOI: doi: 10.1016/j.lithos.2014.05.002
Reference: LITHOS 3272

To appear in: *LITHOS*

Received date: 16 August 2013
Revised date: 29 April 2014
Accepted date: 1 May 2014

Please cite this article as: Osterhus, L., Jung, S., Berndt, J., Hauff, F., Geochronology, geochemistry and Nd, Sr and Pb isotopes of syn-orogenic granodiorites and granites (Damara orogen, Namibia) – arc-related plutonism or melting of mafic crustal sources?, *LITHOS* (2014), doi: 10.1016/j.lithos.2014.05.002

Geochronology, geochemistry and Nd, Sr and Pb isotopes of syn-orogenic granodiorites and granites (Damara orogen, Namibia) – arc-related plutonism or melting of mafic crustal sources?

Osterhus, L.[1], Jung, S.[1*], Berndt, J.[2], Hauff, F.[3]

[1] Fachbereich Geowissenschaften
Mineralogisch-Petrographisches Institut
Universität Hamburg
20146 Hamburg, Germany
email: stefan.jung@uni-hamburg.de

[2] Institut für Mineralogie
Universität Münster
Corrensstraße 24
48149 Münster, Germany
email: jberndt@uni-muenster.de

[3] IFM-GEOMAR
Research Division 4, Dynamics of the Ocean Floor
Wischhofstrasse 1-3
24148 Kiel, Germany
email: fhauff@geomar.de

* corresponding author

Abstract

The Gawib pluton (Damara Belt, Namibia) consists of two main intrusive rock types; magnesian, calc-alkaline, mostly metaluminous hornblende- and titanite-bearing granodiorites and magnesian to ferroan, metaluminous to slightly peraluminous calc-alkaline granites. Uranium-Pb zircon data obtained on the granodiorites gave concordant ages of 548.5±5.6 Ma indicating that the pluton belongs to the early syn-orogenic magmatism in the Damara orogen. Major and trace element variations indicate that fractional crystallization was the major rock-forming mechanism for the granodiorites. In the absence of high-precision geochronological data, the granites may represent more advanced fractionation products of the granodiorites although distinct Ba-Sr-Rb relationships preclude a direct derivation of the granites from the exposed granodiorites. If the granites originated by extensive fractional crystallization from similar granodiorites, they can only be derived from high-Ba, high-Sr, low-Rb granodiorites. Crustal contamination was also important in the petrogenesis of both rock types (granodiorites: ε $Nd_{(init.)}$: -7 to -13; $^{87}Sr/^{86}Sr_{(init.)}$: 0.708-0.713; granites: ε $Nd_{(init)}$: -14 to -18; $^{87}Sr/^{86}Sr_{(init.)}$: 0.712-0.726). In contrast to the granodiorites, the granites show more radiogenic $^{87}Sr/^{86}Sr$ ratios and less radiogenic ε Nd values indicating different contaminants for both rock types. ε Nd vs. MgO relationships imply some genetic link to isotopically unevolved quartz diorites similar to those observed at the Palmental complex. This pluton, however, is located c. 80 km NE from the Gawib pluton and probably cannot be viewed as the direct source of the Gawib granodiorites. If such a relationship is allowed, the granodiorites must be viewed as hybrid rocks containing a juvenile component because they were derived from unevolved quartz diorites by fractional crystallization. In addition, AFC processe have also played a role implying that the granodiorites contain also a reprocessed crustal component. Alternatively, comparison with experimentally derived melts imply that the granodiorites are generated by dehydration melting of a mafic, amphibole-bearing lower crustal source. Chemical parameters of the granodiorites compared to experimental results indicate high temperatures of c. 1040^{o}C. Zirconium saturation temperatures obtained on

the most primitive samples gave c. 830°C whereas apatite saturation temperatures obtained on the same samples give temperatures of c. 960-980°C; the latter seems to be a more reliable temperature estimate. Interpretation of geochemical and isotope data from the complex suggest that the early synorogenic Pan-African igneous activity in this part of the Damara Belt was a high-temperature intra-crustal event. In contrast to igneous processes along active continental margins that produce also intermediate plutons with calc-alkaline affinities, this igneous event was not a major crust-forming episode and the granodiorites represent mostly reprocessed crustal material.

Keywords: Pan-African, Damara belt, granodiorite-granite, partial melting, Sr-Nd-Pb isotopes, U-Pb zircon chronology

1. Introduction

Continental crust has an estimated granodioritic composition and is vertically stratified from a less evolved, mafic lower crust to a more evolved, felsic upper crust (Rudnick and Fountain, 1995). A key question, central to understanding the evolution of continental crust, concerns the origin of intermediate to silicic magmatic rocks that dominate the upper crust. There is general agreement that intermediate magmas form either by differentiation of primary, mantle-derived magmas during cooling and crystallization (e.g. Gill, 1981; Grove and Kinzler 1986; Musselwhite et al., 1989; Rogers and Hawkesworth, 1989) or by partial melting of older crustal rocks (e.g. Atherton and Petford, 1993; Tepper et al., 1993; Wolf and Wyllie, 1994; Rapp and Watson, 1995; Petford and Atherton, 1996; Chappell and White, 2001). These processes can occur together to generate magmas of hybrid origin through assimilation and mixing (e.g. De Paolo, 1981). Evidence for crustal assimilation and mixing of melts from different sources is common in a wide range of tectonic settings (Grove et al., 1988, 1997; Musselwhite et al., 1989).

In the Proterozoic Damara orogen of Namibia, Sr, Nd, Pb and O isotope data allow distinction of several different granite suites. These suites include (i) synorogenic S-type granites that originated by partial melting of upper crustal metasedimentary rocks (Haack et al., 1982; Hawkeswort et al., 1986; McDermott et al., 1996; Jung et al. 2000, 2001), (ii) synorogenic granites that were derived by melting of meta-igneous Proterozoic basement rocks (Hawkesworth et al., 1986; McDermott et al., 1996, Jung et al., 2003) and (iii) late-orogenic A-type granites; some of them represent mixtures between moderately depleted meta-igneous source rocks and a component from the lithospheric mantle (Jung et al., 1998; McDermott et al. 2000). In addition, melting of mafic lower crust yielded early synorogenic quartz diorites to granodiorites (van de Flierd et al., 2003; Jung et al., 2002; 2009). In this study, new LA-ICP-MS U-Pb zircon data and major and trace elements as well as Nd, Sr and Pb isotopes of the granodiorites and granites of the Gawib pluton (Namibia) are interpreted to constrain their sources, melting conditions and the role of AFC processes. This small-scale pluton most likely belongs to the synorogenic granites derived by melting of meta-igneous Proterozoic basement rocks mentioned above.

2. Geological setting and petrography

The Damara orogen of Namibia represents a deeply eroded section through a Pan African mobile belt. It can be divided into the north-south extending Kaoko belt and the northeast-southwest trending intracontinental Damara belt (Miller, 1983, 2008; Fig. 1). This intracontinental branch has been subdivided into a Northern Zone (NZ), a Central Zone (CZ) and a Southern Zone (SZ) based on stratigraphy, metamorphic grade, structure and geochronology (Miller, 1983, 2008). The Central Zone (75.000 km²) is characterized by a large number of intrusions (96 % granites, 4 % diorites, tonalites and granodiorites) in which the majority intruded between c. 570 and 460 Ma (Miller, 1983; 2008). Pre-Damara basement gneisses with radiometric ages ranging from 2.0 Ga to 1.2 Ga are covered by the Neoproterozoic Nosib Group which can be

divided into the Etusis Formation (quartzose sandstones and arkoses) and the Khan Formation (quartzites, schists and calc-silicate rocks). These formations are overlain by the metasedimentary Swakop Group which can be divided into the Rössing Formation (marble, quartzite, conglomerate and schists), the Chuos Formation (metamorphosed glaciogenic diamictites, banded iron-stones, marble, quartzite), the Karibib Formation (marble, schists and calc-silicate rocks) and the Kuiseb Formation (Al-rich metapelites, carbonates, calc-silicate rocks, quartzites and conglomerates).

Puhan (1983) determined temperatures of 555 to 645°C and pressures of 3 ± 1 kbar on impure marbles for the peak of metamorphism in the Central Zone. Similar conditions (c. 570 - 650°C) have been determined through O-isotope analysis on metasedimentary rocks and orthogneisses (Hoernes and Hoffer, 1979). More recent work indicated higher temperatures ranging from 700 to 750 °C at pressures between 4 and 6 kbar (Masberg et al., 1992; Jung, 2000; Jung and Mezger 2002). High-grade metamorphism in the Central Zone occurred between 540 and 500 Ma (Jung, 2000; Jung and Hellebrand, 2006; Jung et al., 2009). In the south-east, the Okahandja Lineament Zone separates the Central Zone from the Southern Zone (Fig.1). In the Southern Zone, regional metamorphism is characterized by a Barrovian-type sequence with a general increase in the metamorphic grade from south to north, with pressures up to 8 kbar at maximum temperatures of 600^{o}C. Intrusion of large volumes of granitic rocks are absent even in the highest grade zone.

The foliated granodioritic to granitic Gawib pluton forms a teardrop-like intrusion and has a dimension of approximately 120 km² (Fig. 2; Miller, 2008). It is located in the transition zone between the SZ and the southern CZ in which the latter is mainly characterized by basement rocks, high-grade metasedimentary rocks and syn-orogenic granites (Fig. 2). The pluton consists mainly of grey granodiorites with plagioclase, quartz, alkali feldspar (microcline and orthoclase), hornblende and biotite in decreasing abundance. The pluton is transected by reddish to light-grey granitic dikes consisting of alkali feldspar (microcline and orthoclase), quartz, plagioclase and biotite. Accessory phases include titanite, apatite, zircon, secondary muscovite and ore

minerals, most likely magnetite but chemical analyses are not available. Plagioclase is unzoned and shows polysynthetic twinning. Alkali feldspar shows microcline twinning with partly perthitic exsolution. Hornblende form euhedral to subhedral crystals often associated with aggregates of titanite and ore minerals. Sericitization of feldspar and chloritization of biotite is rarely observed. Quartz and feldspar show 120° grain boundaries suggesting static annealing at moderate high temperatures.

3. Analytical techniques

Zircon separates for U-Pb dating were prepared by sieving the samples through a 100-250 mesh fraction, followed by purification by magnetic separation. Subsequently, the mineral fractions were separated by methylene iodide and handpicking, which produced high-purity separates. The separated zircons were fitted into epoxy resin for U-Pb measurements via a LA-ICP-MS (laser ablation inductive coupled plasma mass spectrometer) from type UP193HE, Element 2. Details on the analytical protocol are given in Jung et al. (2012).

Whole rock powders were prepared using a jaw crusher, a rod mill and an agate mortar. Major and trace elements (except for REE) were measured on fused lithium-tetraborate glass beads using standard XRF technique at the Universität Hamburg using a PanAnalytical MagixPro X-ray fluorescence spectrometer. Rare earth elements of some samples (“M” samples) were carried out by ICP-AES techniques at the Universität Marburg following separation of the matrix elements by ion exchange (Heinrichs and Hermann, 1990). Loss on ignition (LOI) was determined gravimetrically after heating the samples at 1,000°C for 3 h (Lechler and Desilets, 1983). Trace elements abundances of other samples (“GW” samples) were measured by Actlabs via a Perkin Sciex ELAN ICP-MS. Accuracy was controlled by repeated measurements against international and in-house standards and the results are in good agreement with the recommended values.

For the Rb-Sr and Sm-Nd whole rock isotope analyses, the samples were digested in concentrated HF-HNO_3 in 3-ml screw-top Teflon vials inside Krogh-style Teflon bombs at 200°C for 2 days. After the complete dissolution, the samples were dried down and redissolved in 2.5 N HCl. Strontium and REE were separated by using standard cation exchange columns with a Dowex AG 50 W-X 12 resin using 2.5 N HCl for Sr and 6 N HCl for the REE. Neodymium was separated from the other REE by using HDEHP-coated Teflon columns and 0.12 N HCl for Nd. Isotope analyses were carried out at the Institut für Mineralogie (Universität Münster) using thermal ionization mass spectrometry with a Finnigan Triton MC-TIMS operating in the static mode. Neodymium was run on Re double filaments. Neodymium isotopes were normalized to $^{146}Nd/^{144}Nd = 0.7219$. The total procedural blank for Nd was <40 pg and is considered to be negligible. Repeated measurements of the La Jolla Nd standard gave $^{143}Nd/^{144}Nd = 0.511859 \pm 0.00007$ (2σ; n = 10). Strontium was run on W single filaments. The reproducibility of the Sr standard (NBS 987) is $^{87}Sr/^{86}Sr = 0.710213 \pm 0.000007$ (2σ; n = 10) and the fractionation was corrected to $^{86}Sr/^{87}Sr = 0.1194$. Uncertainties in the $^{87}Sr/^{86}Sr$ and $^{143}Nd/^{144}Nd$ are reported in the last two digits.

Between 40 and 50 mg of high-purity K-feldspar separates were washed with a mixture of 3:1 HCl/HNO_3 to remove surface contamination and were subsequently rinsed twice with ultrapure water. Then the separates were leached two times in a mixture of concentrated HF/HNO_3, resulting in a weight loss of c. 60%. Thereafter the feldspars were dissolved in concentrated HF and after evaporation redissolved in 2.5 N HCl and 1 N HBr and loaded onto 100 µl Teflon microcolumns filled with Dowex AG 1 X 8 (100-200 mesh) anion exchange resin. Lead was extracted and purified (in a second column pass) using conventional HBr/HCl techniques and was loaded onto Re single filaments following the H_3PO_4-silica gel method of Cameron et al. (1969) using the silica recipe of Gerstenberger and Haase (1997). Lead isotope analyses were carried out on a VG Sector 54 MC-TIMS (Münster) and a Finnigan MAT 262 MC-TIMS (GEOMAR) and were corrected for mass fractionation by 0.11% per amu on both instruments.

4. Geochronology

Table 1 gives U-Pb data for zircon from the Gawib pluton and Fig. 3 shows U-Pb ages for the different zircon fractions from granodiorite sample M 89. The zircon grains with sizes between 80 and 350 µm often exhibit concentric zonation patterns likely indicating a magmatic origin for these grains**.** Several grains yielded a concordant U-Pb age of 548.5 ± 5.6 Ma which is considered to represent the intrusion age (Fig. 3a). Some other analyses are discordant and, when forced through zero, give an upper intercept of 537 ± 25 Ma (Fig. 3b). These anaylses have likely undergone recent Pb loss. Other fractions yielded a concordant U-Pb age of 1935 ± 11 Ma that could be interpreted as the age of the underlying basement (Fig. 3c). This view is consistent with the interpretation of a number of discordant data points yielding an upper intercept of 1961 ± 29 Ma and a lower intercept of 545 ± 20 Ma (Fig. 3d). One zircon analyses yielded an U-Pb age of 2786 ± 17 Ma (Table 1) representing the oldest U-Pb zircon age measured so far in igneous rocks from the Damara orogen. We interpret this grain as an inherited grain from the underlying basement.

5. Geochemistry

5.1. Major- and trace elements

The Gawib granodiorites have SiO_2 concentrations between 63.6 wt.% and 66.8 wt.% (Table 2). They are metaluminous with A.S.I. (alumina saturation index) values ranging from 0.88 to 1.00 and have moderate high TiO_2 (0.30-0.83 wt.%), MgO (0.8-1.9 wt.%), $Fe_2O_{3\ total}$ (3.1-6.0 wt.%) and Al_2O_3 contents (14.0-16.5 wt.%). Contents of CaO (2.9-4.6 wt.%), Na_2O (3.1-4.7 wt.%) and K_2O abundances (2.7-4.1 wt.%) are similar to other granodiorites from the Damara orogen with similar SiO_2 contents (Fig. 4). The Ba and Sr contents of the granodiorites are high (Ba: 601-

1319 ppm; Sr: 560-939 ppm) whereas Rb contents are only moderately high (Rb: 107-212 ppm) (Fig. 5). Consequently, Rb/Sr ratios (0.13-0.33), Sr/Ba ratios (0.64-1.16) and Rb/Ba ratios (0.09-0.27) are low. The granodiorites are enriched in REE with total REE abundances ranging from 165 to 400 ppm (Table 2). Rare earth element (REE) distributions show an enrichment of LREE for the granodiorites with La_N/Sm_N ratios ranging from 3.7 to 5.8. Heavy Rare Earth Element abundances are also enriched with Gd_N/Yb_N ratios between 1.8 and 3.1 (Fig. 6).

The granites have higher SiO_2 contents between 70.7 and 76.0 wt.% and are weakly peraluminous (ASI: 1.00-1.05). Relative to the granodiorites, the granites have lower abundances of TiO_2 (0.05-0.1 wt.%), MgO (0.1-0.4 wt.%), $Fe_2O_{3\ (total)}$ (0.6-1.7 wt.%) and Al_2O_3 (12.8-14.5 wt.%). The granites have CaO contents between 0.7 and 2.1 wt.%, Na_2O contents between 3.0 and 3.6 wt.% and K_2O contents between 4.1 and 5.9 wt.% (Fig. 4). For the granites, there is considerable overlap in Ba and Rb abundances (146-1108 ppm Ba and 157-281 ppm Rb). Strontium abundances are lower relative to the granodiorites (84-523 ppm) (Fig. 5). Rb/Sr and Rb/Ba ratios increase with increasing SiO_2 and therefore the granites have higher Rb/Sr and Rb/Ba ratios than the granodiorites (Rb/Sr: 0.3-3.3; Rb/Ba: 0.2-1.9). Sr/Ba ratios are broadly similar to the lowest values observed in the granodiorites (Sr/Ba: 0.5-0.7). The granites have lower total REE contents than the granodiorites between 40 and 91 ppm (Table 2). They are also enriched in LREE ($La_N/Sm_{N:}$ 5.1-6.2) whereas some samples show depletion of MREE and/or enrichment in HREE leading to variable Gd_N/Yb_N ratios between of 0.8 and 2.1 (Fig. 6).

5.2. Nd, Sr and Pb isotopes

The results of the Sr, Nd and Pb isotope analyses are reported in Table 3. The most primitive granodiorites have an unradiogenic Nd isotopic composition with initial ε Nd values of c. – 8 and moderately radiogenic initial $^{87}Sr/^{86}Sr$ ratios of 0.708-0.709 (Fig. 7). The most evolved granodiorite has an initial ε Nd value of -13 and a Sr isotope composition of 0.713. For the granites, initial ε Nd values are more unradiogenic with ε Nd values ranging from -18 to -14 and

$^{87}Sr/^{86}Sr$ ratios of 0.712-0.726 (Fig. 7). The $^{206}Pb/^{204}Pb$ and $^{207}Pb/^{204}Pb$ ratios (Fig. 8) of the granodiorites and granites range from 17.45 to 17.92 and 15.56 to 15.68, respectively (Table 3). The $^{208}Pb/^{204}Pb$ ratios range from 38.00 to 38.71. In $^{207}Pb/^{204}Pb$ vs. $^{206}Pb/^{204}Pb$ space and $^{208}Pb/^{204}Pb$ vs. $^{206}Pb/^{204}Pb$ space, both suites plot above the Pb evolution curve of Stacey and Kramers (1975) (Fig. 8) indicating derivation from a source with a higher U/Pb and Th/Pb ratio than the reference source.

6. Discussion

6.1. Fractional crystallization and AFC processes

A general fractional crystallization trend is indicated by decreasing TiO_2, MgO, FeO, CaO, Al_2O_3, P_2O_5, V, Ni, Cr, Sc, Sr, Ba and Y, Nb, Ta, Hf, Zr, Th (not shown) concentrations and increasing Na_2O, K_2O, Pb, Rb (and U) concentrations with increasing SiO_2 (Fig. 4 and 5). These trends can be interpreted to indicate fractionation of amphibole, plagioclase, Fe-Ti-oxides, apatite and zircon. It seems also reasonable to assume that in granitoid systems feldspars would be the most important minerals in any fractionation scheme, and the size of the negative Eu anomaly (expressed as Eu/Eu*) together with low Sr concentrations would be a measure of the degree of feldspar fractionation. The most primitive granodiorites have negligible negative Eu anomalies which are unrelated to the Sr concentration. Others have lower Sr abundances and more pronounced negative Eu anomalies although the correlation is poor. For the granodiorites, La and Y abundances together with TiO_2 decrease with decreasing MgO suggesting modification of these parameters during fractional crystallization. Depletion of LREE and HREE during fractional crystallization is compatible with fractionation of mineral phases e.g. amphibole or titanite which may concentrate LREE and HREE (e.g. Jung and Hellebrand, 2007). In addition, apatite which may prefer LREE may have contributed to the decrease in LREE which is also compatible with the decrease in P_2O_5 with increasing SiO_2.

Among the granites, a positive correlation between Eu anomaly and Sr concentration suggest removal of plagioclase during fractionation. The most primitive granite has a slightly positive Eu anomaly and the highest Sr concentration indicating some accumulation of plagioclase (Fig. 9a). To explain the decrease in LREE and HREE, the diminishing Eu anomaly and the ocurrence of a concave-upward REE pattern at low total REE contents, a complex fractionating mineral assemblage must be envisaged which may has included apatite, titanite and hornblende. Fractionation of hornblende is also compatible with petrographic observations and Sr-Rb variations (see below). Strontium-Rb variations can be used to place semi-quantitative constraints on the fractionated mineral assemblage (Fig. 9b) and were calculated using a Rayleigh fractionation model. Application of this model suggests that the fractionation assemblage consists of hornblende (ca. 20 wt. %), plagioclase (ca. 70 wt.%) and K-feldspar (ca. 10 wt.%) in the case of the granodiorites. For the granites, fractionation may involve plagioclase (ca. 65 wt.%) and K-feldspar (ca. 35 wt.%). Obviously, fractionation of biotite was not important which is also consistent with the increase in Rb with increasing SiO_2.

For the granodiorites, some major and trace elements show variations that can probably not attributed to fractional crystallization processes alone. It is possible that rocks similar to coeval quartz diorites from nearby complexes are parental to the granodiorites although the Gawib pluton lack those mafic rocks. Variations in Al_2O_3, K_2O or TiO_2 (Fig. 4) or Ba, Rb, Sr and Ni (Fig. 5) imply that a range of possible quartz diorites may exist at depth and that these variations are related to heterogeneity of the sources. Similarly, for the granodiorites alteration seems not to have played a major role and AFC processes (see below) as a major cause of this variation can be ruled out because major element and some trace element abundances (except Sr and Ba) observed in the granodiorites are already similar to average continental crust.

Strontium, Nd and Pb isotope compositions are heterogeneous and before considering the origin of the granodiorites and granites in detail it is necessary to investigate the likely reasons for this isotope heterogeneity. Initial $^{87}Sr/^{86}Sr$ ratios and ε Nd values show systematic behavior with respect to major element chemistry in which initial $^{87}Sr/^{86}Sr$ ratios (not shown)

increase while initial ε Nd values decrease with decreasing MgO concentration (Fig. 10). Similarly, the granodiorites show a range of Nd model ages from 1.5 to 2.5 Ga which are unlikely to result from source heterogeneity. It is more likely that this range of Nd model ages is the result of assimilation of pre-existing ancient lower crust. These features indicate that during crystal fractionation processes linked to assimilation of country rock material substantially modified the isotopic composition. Processes of crustal assimilation can be illustrated by using radiogenic isotope systems with different properties (i.e. Sr and Nd). The composition of the granodiorites and granites and different Damara country rocks (a basement gneiss collected in the vicinity of the Gawib pluton, Pre-Pan African Proterozoic basement from the Kaokoveld and metasedimentary rocks from the Khan and Etusis formation; McDermott and Hawkesworth, 1990; Jung 2005; Seth et al., 2002) are shown in a diagram of $^{87}Sr/^{86}Sr$ vs. ε Nd (Fig. 11). As a simplification, it can be suggested that such lithologies are the most fusible parts of a crustal segment and thus are most likely involved in any assimilation scenario. A potential parental granodiorite should have high Sr contents (700 - 900 ppm; Fig. 5), high Nd contents (c. 40 - 50 ppm; Table 2) and a comparatively unradiogenic Sr and Nd isotopic composition. From Fig. 11 it can be seen that for the majority of the granodiorites the negative correlation between Sr and Nd isotope composition is best monitored by using a sample from the Proterozoic basement from the Kaokoveld (Seth et al., 2002) as the contaminant. The amount of assimilation can be estimated to be 30% in which the value of r (r=ratio of assimilation to fractionation) was set at 0.6. Using higher values of r results in higher F values (F=fraction of melt remaining) greater than 0.85, implying assimilation of only a small fraction of crustal material. In contrast to previous estimates about the ratio of mass assimilated to mass fractionated ($r < 1$; DePaolo, 1981) higher values of r ($r > 2$; Reiners et al., 1995) especially in the early stages may be possible. High values of r further imply that assimilation took place at high temperatures and hence at deeper levels within the crust. However, r values greater than 1 cannot be successfully applied to the AFC model of DePaolo (1981).

The AFC model applied to the granodiorites does not reproduce the isotope composition of the granites. The granites are distinctly more radiogenic in $^{87}Sr/^{86}Sr$ and this increase in Sr isotope composition requires some interaction either with rocks similar to the basement gneiss collected nearby or with overlying metasedimentary rocks (Fig. 11). The Pb isotope composition is particularly susceptible to extreme changes during AFC as a result of the high concentration of Pb in metasedimentary crustal rocks relative to mafic or intermediate rocks and small compositional differences in the contaminant can be responsible for significant changes in Pb isotope composition. Unfortunately, Pb isotope data are not available from basement gneisses. It is interesting that for the granodiorites $^{206}Pb/^{204}Pb$ isotope compositions are positively correlated with Nd isotope compositions indicating that increasing contamination is accompanied by decreasing ε Nd, increasing $^{87}Sr/^{86}Sr$ but decreasing $^{206}Pb/^{204}Pb$ ratios (Fig.12). The latter implies involvement of a lower crustal contaminant with a low U/Pb ratio. For the granites, the opposite is observed; decreasing ε Nd is accompanied by increasing $^{206}Pb/^{204}Pb$ ratios. This suggests that AFC processes that modified the isotope composition of the granites involved an endmember with low MgO, high SiO_2, comparatively unradiogenic Nd but radiogenic Sr isotope compositions and radiogenic $^{206}Pb/^{204}Pb$ ratios (Fig. 12). This inferred contaminant must have a high μ and a high κ value. Such rocks constitute potentially the underlying pre-Damara basement of the Central Zone of the Damara orogen (Jung et al., 2003) or metasedimentary rocks derived from the basement (McDermott and Hawkesworth, 1990).

6.2. Partial melting processes and possible sources of the granodiorites and granites

The generation of mafic to intermediate magmas (quartz diorites, granodiorites) is widely accepted as an important component in studies concerned with crustal growth and intermediate magmas forming sometimes voluminous plutonic complexes are an important component of many orogenic belts. As a general feature in these arc-related belts, mafic magmas may come directly from the mantle and may be interpreted to serve as heat sources to melt crustal material

(e.g., Holden et al. 1987). On the other hand, mafic magmas may undergo pure crystal fractionation to yield more evolved magma, negating the need for crustal contributions to produce felsic magma (Sisson et al. 1996 ; Coleman and Glazner 1997; Ratajeski et al. 2001; Wenner and Coleman 2004). In the former case, no new continental crust is formed; in the latter, the more evolved magmas are new additions to the continental crust. Between these two endmembers are intermediate processes whereby juvenile mafic magma can produce intermediate to felsic magmas through a combination of crystal fractionation, assimilation of continental crust, and hybridizing with more silicic melts (e.g., DePaolo 1981; Reid et al. 1983; Kistler et al. 1986 ; Frost and Mahood 1987; Barbarin, 2005; Dorais et al. 1990 among many others). The Mesozoic arc-related plutons of the western US may serve as a general example; here, models involve either simple two-component mixing of a depleted mantle component with an old metasediment component to produce ‘‘evolved’’ whole rock isotopic compositions or involve mafic magmas formed by melting of an enriched subcontinental lithospheric mantle followed by pure crystal fractionation. Many of the mafic to intermediate rocks in the Sierra Nevada batholith represent juvenile additions to the crust at the time of emplacement (Coleman et al., 1992; Coleman and Glazner, 1997), however Nelson et al. (2013) have shown that assimilation of aged continental crust into a mantle-derived precursor is also a viable process to generate mafic to intermediate magmas. The granodiorites are associated with low-silica (dioritic) and high- silica (granitic) rocks that are the same age (Coleman et al., 1995; Ratajeski et al., 2001), and all of these rock types may share a genetic origin (Frost and Mahood, 1987).

The Gawib pluton from the Damara orogen in Namibia has an intermediate composition similar to granodiorites found in the Sierra Nevada batholith (Figs. 4, 5, 6 and 13). Intermediate plutonic rocks from the Sierra Nevada batholith are of particular importance here because one component, the Tuolumne igneous suite served as a key example in defining magnesian calc-alkaline rocks (Bateman and Chappell, 1979; Frost et al. 2001). The overall situation found in the Sierra Nevada batholith with an areal extent of ca. 32000 km^2 is similar to what is observed in the area of the Gawib pluton although the area around the Gawib pluton is considerably smaller

(ca. 1600 km^2) even when the coeval quartz diorites are included. Here, the granodiorites are associated with granites and the coeval quartz diorites form the Goas, Okongava and Palmental areas (Jung et al., 2002; unpubl.) can be viewed as the more mafic endmembers. In the following we will discuss first the possibility that the Gawib granodiorites have a similar derivation to arc-related granodiorites such as those found in the Sierra Nevada batholith. Figures 4 and 5 indicate that the Gawib granodiorites have a major and trace element composition similar to granodiorites from the Sierra Nevada batholith. However, Sr-SiO_2 relationships indicate that there are two types of quartz diorites; high-Sr diorites with > 600 ppm Sr and low-Sr diorites with < 600 ppm Sr (Fig. 5). It is important to note that the high-Sr quartz diorites are confined to the Palmental complex (Jung unpubl., Fig. 2) whereas diorites from the Goas and Okongava areas constitute the low-Sr diorites. Similarly, Fig. 9a and 10 also imply that if some quartz diorites are parental to the Gawib granodiorites, it must be the Palmental diorites but not the Goas and Okongava diorites. More importantly, in the Palmental complex, some quartz diorites have comparatively radiogenic Nd (ε Nd: ≈ -3) and unradiogenic Sr ($^{87}Sr/^{86}Sr$: ≈ 0.706) isotope composition whereas the Goas and Okongava quartz diorites have strongly evolved isotope compositions (ε Nd: ≈ -9 to -15; $^{87}Sr/^{86}Sr$: ≈ 0.709-0.712). Thus, although the quartz diorites in the central Damara orogen are not spatially associated with the Gawib granodiorites, some samples from the Palmental complex have the appropriate composition to be parental to the Gawib granodiorites. In this case, the Palmental quartz diorites and the Gawib granodiorites would be connected by a common AFC process in which the parental quartz diorites were derived from an aged lithospheric mantle. In this case, the lithospheric mantle gained its enrichment in Sr and Nd isotope composition either through source contamination or mantle metasomatism. The quartz diorites would then represent juvenile additions to the continental crust but the granodiorites have a hybrid origin containing both, new crustal material and reprocessed crustal rocks.

Although the AFC model presented above seems to be a plausible scenario to explain the elemental and isotopic composition of the Gawib granodiorites, some points require

consideration. First, the idea that some of the Plamental quartz diorites are parental to the granodiorites can be questioned because such rocks are not known from the Gawib pluton and the Palmental complex is situated ca. 80 km away from the Gawib pluton. Second, an arc-related scenario comparable to the Sierra Nevada batholith, although compatible with the new U-Pb zircon ages, is probably unlikely due to the limited occurrence of intermediate plutonic rocks in the area and the small scale of the Gawib pluton. It is therefore also possible that the granodiorites are primary melts generated by melting of mafic lower crust. Many plutonic complexes containing igneous rocks more mafic than granite are generated through partial melting of pre-existing meta-igneous rocks and some of these melts are high K-granodiorites, granites and tonalites. Roberts and Clemens (1993) argued that, because of their low K_2O concentrations, common metabasaltic sources can generally be considered as unsuitable sources. However, early experimental investigations (Helz, 1976) indicated that these high-K (> 3 wt. % K_2O at 65 wt. % SiO_2) magmas can only be derived by melting of hydrous, high-K calc-alkaline mafic to intermediate metamorphic rocks in the crust. Subsequent experimental studies have shown that the nature of experiment (fluid-present vs. fluid-absent) also strongly influences the composition of the melt and residuum during partial melting of basaltic composition at mid- to lower crustal pressures (Beard and Lofgren, 1991; Wolf and Wyllie, 1994; Rapp and Watson, 1995). Depending on bulk composition, fluid-absent partial melting of amphibolite yields 10-60% melt at temperatures of 900-1100^{o}C whereas fluid-present partial melting yields similar amounts of melt at lower temperatures between 850-900^{o}C. Melt compositions are different in which liquids produced by fluid-absent melting are more mafic (quartz-dioritic to granodioritic and tonalitic) whereas liquids produced by fluid-present melting are rich in SiO_2 and Al_2O_3 but low in FeO and MgO (i.e. granitic).

The most mafic granodiorites of the Gawib pluton have chemical features that typify partial melts of basaltic rocks. They have intermediate SiO_2 and high Al_2O_3 contents and high LREE concentrations and moderate low HREE concentrations. Na_2O/K_2O ratios are > 1. The majority of the granodiorites have high Sr and Ba abundances and negligible negative Eu

anomalies suggesting that the source was feldspar-free or feldspar was melted to a large extend during generation of the parental granodiorites. The lack of HREE and Y depletion indicates a garnet-absent source. The most mafic granodiorites of the Gawib pluton have K_2O > 2.0 wt. %, MgO < 2 wt. %, CaO > 2.5 wt. %, FeO_{total} > 3 wt. % and TiO_2 < 1.0 wt. %. These features are monitored by high temperature melting experiments (c. 1000^oC) using common amphibolites as the starting material (Beard and Lofgren, 1991, Wolf and Wyllie, 1994, Rapp and Watson, 1995). It has been argued that entrainment of peritectic phases may yield magmas more mafic than granite (Clemens et al., 2011; Clemens and Stevens, 2012). In this paper, we presented also data from coeval nearby quartz diorites although the Gawib complex lack such rocks. Major and trace element evidence suggest that such quartz diorites may be the parental melts and both rock types are connected through fractional crystallization processes although the linear relationships in major and trace element abundances can also be produced by entrainment of peritectic phases. From experimental studies and phase petrology, partial melting of amphibolites or mafic granulites yields clinopyroxene, orthopyroxene and garnet as peritectic phases; however, none of these minerals occur in the quartz diorites or granodiorites. In addition, HREE systematics rule out a significant contribution of garnet or clinopyroxene during melting. Finally, entrainment of peritectic phases must result in considerable scatter in Nd-Sr space and would not yield linearly correlated Sr-Nd isotope data which are more compatible with AFC processes.

Based on a comparison with melting experiments using TiO_2 as the most incompatible major element (Fig. 14a), the most primitive granodiorites from the Gawib pluton plot either in the field of experimental melts generated by **"**wet" melting of metabasaltic sources (Beard and Lofgren, 1991) or in the field of melts derived by fluid-absent melting of amphibolite sources (Rapp and Watson, 1995). In the case of the Gawib granodiorites, fluid-present melting can be considered as an implausible process to generate mobile granodioritic magmas because the Al_2O_3 contents are too high and FeO and MgO are too low relative to the Gawib granodiorites. Melts derived by fluid-absent melting of amphibolites (Beard and Lofgren, 1991) seem to have

higher TiO_2 abundances at a given SiO_2 content (Fig. 14a). In a similar approach, Rapp and Watson (1995) used various meta-basaltic sources to generate intermediate magmas through fluid-absent melting. Notably, they used an alkali basaltic source rock enriched in TiO_2 and K_2O that yielded high-K_2O magmas (> 2 wt. % K_2O at 65 wt. % SiO_2) with appropriate TiO_2 contents (ca. 1 wt. % TiO_2 at 65 wt. % SiO_2). It is important to note, that the generation of intermediate magmas with slightly elevated TiO_2 contents is independent of the TiO_2 content of the source material since both, the source materials from Rapp and Watson (1995) and Beard and Lofgren (1991) had similar TiO_2 contents of 0.72 - 2.06 wt% and 0.60 - 1.74 wt%, respectively. Similarly, the match between experimental melts and the Gawib granodiorites in Al_2O_3, FeO and MgO is good. The alkali basaltic source rock used by Rapp and Watson (1995), however, has a more differentiated composition relative to the other tholeiitic sources with lower CaO contents, hence the match between experimental melts and the Gawib granodiorites in terms of CaO abundances is poor. A comparison of FeO (ca. 6 wt. %), MgO (ca. 2 wt. %) and TiO_2 (ca. 0.8 wt. %) abundances between experimental melts and the Gawib granodiorites suggest temperatures between 900 and 1100^{o}C (Fig. 14b). Constraints on the melting temperature can also be obtained by plotting chemical parameters of experimental melts against their experimental temperature and by comparing these chemical parameters with those of the most primitive granodiorites. Accepting that the source is broadly similar to those used in the dehydration melting experiments of Rapp and Watson (1995), the most primitive granodiorites have Mg+Fe+Ti values (in cation percentages) of c. 0.13 indicating a temperature of c. 1040 +30/-15^{o}C (Fig. 15). Similarly, these samples have Al/(Mg+Fe) ratios of c. 1.3 (not shown here) which point to temperatures of c. 1070^{o}C. Although there is probably a relatively large uncertainty with this approach, high temperatures are indicated.

The temperature at which a mafic melt separated from its source may be estimated from its P_2O_5 concentration, using the apatite solubility expression of Harrison and Watson (1984). This approach assumes that the melt formed in equilibrium with residual apatite and has not undergone subsequent modification by processes related to fractional crystallization or

assimilation. The first requirement may be satisfied during melting, especially at low degrees of melting, but the second requirement is more difficult to evaluate. However, the most mafic quartz diorites have the most primitive isotopic composition indicating less modification by AFC processes. For these samples P_2O_5 concentrations are between 0.32-0.35 wt%, indicating temperatures of between 960 and 980^{o}C, only slightly lower to those given by the experimental investigations. On the other hand, application of the Zr saturation temperature equation (Watson and Harrison, 1983) indicates a lower temperature of c. 830^{o}C most likely as a result of early zircon fractionation.

At pressures of 10 to 15 kbar calc-alkaline liquids coexist with garnet under both vapor-saturated and -undersaturated conditions (Huang and Wyllie, 1986; Rutter and Wyllie, 1988; Caroll and Wyllie, 1990). None of the granodiorites shows significant HREE depletion (i.e Yb_N < 10) predicted for melts that equilibrated with residual garnet suggesting that they formed alternatively under lower pressures, with less garnet in the residuum or garnet was melted to a large extent during formation of the melts. In any case, the moderate high temperatures required for amphibolite melting restrict this process to the deep crust in which temperatures cannot have exceeded 1100^{o}C at 10-15 kbar which is the thermal stability limit of amphibole in basalt (Green et al., 2010).

In summary, the source rock of the granodiorites is most likely a high-grade metamorphic, medium-K basaltic rock that was melted at moderate high temperatures and pressures in the lower crust. Constraints derived from interpretation of experimental evidence (Beard and Lofgren, 1991; Wolf and Wyllie, 1994; Rapp and Watson, 1995) imply that fluid-absent melting of basaltic material within the lower crust at high temperatures can produce significant volumes of intrusive intermediate partial melts, particular in regions with high heat flow.

6.3 A tentative model for the generation of early syn-orogenic granodiorites

The Damara orogeny included a c. 100 Ma period from 570-480 Ma in which high-T granites intruded the mid-crustal region more or less continuously and on a province-wide scale. For the syn-orogenic granites, the time of intrusion coincides with a first period of high-temperature metamorphism at 540 Ma (c. 700-750^{o}C at 5-6 kbar; Jung and Mezger, 2001; 2003). Such thermal events at mid-crustal regions must be accompanied by even higher temperatures in the lower crust of probably 900-1000^{o}C along a very high geothermal gradient (e.g. Harley, 1998; Brown, 2007; Kelsey, 2008). They almost certainly require a considerable amount of convective heat from the mantle. Numerical thermal modelling also suggests that large-scale crustal melting requires unusually high heat flow (e.g. Petford and Gallagher, 2001; Annen and Sparks, 2002; Dufek and Bergantz, 2005). One feasible explanation to account for the high temperatures at mid crustal levels early in the tectono-metamorphic history could be that the crust contained a high proportion of melt (e.g. in a MASH zone) as a result of intra- and under-plated voluminous mantle melt providing additional heat to melt the crust at mid crustal conditions. Current models indicate that voluminous mantle-derived magmatism contribute both heat and source material in the generation of large-volume felsic magmas in all tectonic environments (e.g. Annen et al., 2006). It is argued that most intermediate to felsic magmas form within, and are extracted from, long-lived crystallizing mush zones periodically fed by mantle-derived magmas. All of these models are based on the MASH hypothesis (melting, assimilation, storage, homogenization; Hildreth and Moorbath, 1988) in which long-lived crystal-melt mush domains are produced when mantle derived mafic underplated and intraplated magmas mix with, and assimilate, local crustal components producing crystal-rich mush chambers that undergo dynamic homogenization as well as periodic magma recharge (Hildreth and Moorbath, 1988). A model that also incorporates aspects of the MASH hypothesis is that of granite formation in deep crust ‘hot zones’ (Annen et al., 2006). This model was developed to explain the genesis of subduction-related felsic magmas, but may also applicable to other tectonic settings where high-T granites occur. According to this model, a relatively high rate of basaltic intraplating can lead to a situation where each successive intrusion adds more heat to the lower

crust than is conducted away. Annen et al. (2006) predicted that within this emerging 'hot zone', ambient temperatures may eventually exceed the solidus temperature of both the basalt and the country rock. Under such conditions, the country rock may partially melt, whereas the basaltic sills will retain a residual melt fraction. This situation favors the generation of mafic to intermediate magmas with hybrid isotope compositions. Interpretation of geochemical and isotope data from the rather small-scale complex suggest that the Pan-African igneous activity in this part of the Damara Belt was not a major crust-forming episode and most rock types represent reprocessed crustal material. The thermal anomaly that acounts for high-temperature melting in the lower crust and subsequent high-temperature/low-pressure regional metamorphism is likely rooted in the lithospheric upper mantle.

7. Conclusions

Rocks from the c. 550 Ma-old Gawib pluton are metaluminous, calc-alkaline, magnesian rocks (Frost and Frost, 2008) in the compositional range of granodiorite to granite. They are enriched in HFSE, Y and REE in which the samples with the lowest SiO_2 have the highest contents of Zr, Nb, Y and LREE. Neodymium and Sr isotope compositions are evolved and Pb isotopes are radiogenic plotting above average Pb growth curves. Although the Gawib granodiorites share many similarities to modern arc-type plutonic rocks (i.e. the Sierra Nevada Batholith), Sr, Nd and Pb isotope systematics are unlike granitic rocks unmodified by AFC processes found in modern continental arcs. A potential genetic link to the coeval isotopically unevolved Palmental quartz diorites located further to the NE is possible, however, if such a genetic link is precluded it is likely that the compositional geochemical and isotope variation of the Gawib granodiorites reflects variable degrees of partial melting of an ancient mafic source at crustal levels. In addition, isotope data imply some modification through limited assimilation of older crust. The range of Nd model ages between 1.5 - 2.5 Ga also indicates involvement of an ancient crustal component.

As pointed out by Frost and Frost (2008), magnesian intermediate to felsic magmas with FeO/(FeO+MgO) < 0.78 at SiO_2 contents ranging from 65-70 wt.% SiO_2 (the range of the Gawib granodiorites) form granitoids that range in composition from calcic to alkali-calcic, metaluminous or peraluminous granodiorite to granite. All these features are shown by the Gawib granodiorites. Frost and Frost (2008) have shown that magnesian granites typically form in arcs and 'post-collisional' environments. The important point is that intermediate igneous rocks in the lower crust in arc settings may be generated by remelting of previously underplated mafic intrusions. They obtain their magnesian signature because the sources are magnesian (Ratajeski et al., 2005; Nelson et al., 2013) and they undergo differentiation under oxidizing (and probably wet) conditions (Frost and Frost 2008). Intrusion and stagnation of primitive basaltic magmas in deep crustal levels may produce fractionated hydrous magmas which may be represented by some isotopically unevolved quartz diorites of the Plamental complex. If no interaction with older crustal rocks occurs during fractionation, the intermediate rocks may have isotope systematics similar to their unevolved mafic sources. On the other hand, combined assimilation-fractional crystallization processes may create hybrid rocks with evolved isotope compostions. On the other hand, remelting of mafic intrusions that intruded much earlier than the Pan-African igneous event yield hydrous mafic magmas with strongly evolved isotope systematics; this situation may apply for the Goas and Okongava diorites and, if the connection of the Palmental diorites with the Gawib granodiorites is precluded, also for the intermediate rocks from the Gawib pluton. The latter point makes a derivation of the Gawib granodiorites by reprocessed mafic crustal material very attractive. The major and trace element data obtained on the granites are compatible with a derivation from high-Sr, high-Ba, low-Rb granodiorites through fractional crystallization. In addition, initial ε Nd values and initial $^{87}Sr/^{86}Sr$ ratios indicate that assimilation of lower crustal rocks was also important for the granites.

Acknowledgements

The authors are grateful to E.Thun and J. Richarz (Hamburg) and H. Baier (Münster) for support

in the laboratory. Especially H. Baier is warmly thanked for her help and advice during the first author´s stay in Münster. SJ thanks Klaus Mezger for hospitality and help over the years. Careful reviews by two anonymus reviewers were helpful in revising the manuscript and are highly appreciated. Nelson Eby is thanked for patient and thorough editorial handling.

References

Annen, C., Sparks, R. S. J. 2002. Effects of repetitive emplacement of basaltic intrusions on thermal evolution and melt generation in the crust. Earth and Planetary Science Letters 203, 937-955.

Annen, C., Blundy, J. D., Sparks, R. S. J. 2006.The genesis of intermediate and silicic magmas in deep crustal hot zones. Journal of Petrology 47, 505-539.

Atherton, M. P., Petford, N. 1993. Generation of sodium-rich magmas from newly underplated basaltic crust. Nature 362,144-146.

Barbarin, B. 2005. Mafic magmatic enclaves and mafic rocks associated with some granitoids of the central Sierra Nevada batholith, California: nature, origin, and relations with the hosts. Lithos 80, 155-177.

Bateman, P. C., Chappell, B. W. 1979. Crystallization, fractionation, and solidification of the Tuolumne Intrusive Series, Yosemite National Park, California. Geological Society America Bulletin 90, 465-482.

Beard, J.S., Lofgren, G.E., 1991. Dehydration melting and watersaturated melting of basaltic and andesitic greenstones and amphibolites at 1, 3 and 6.9 kbar. Journal of Petrology 32, 365-402.

Bohlen S. R., 1987. Pressure-temperature-time paths and a tectonic model for the evolution of granulites. Journal of Geology 95, 617-632.

Boynton, W.V., 1984. Geochemistry of rare earth elements: Meteorite studies. In: Henderson P (Ed), Rare earth element geochemistry, Elsevier, New York, 63-114.

Brown, M. 2007. Metamorphic conditions in orogenic belts: a record of secular change. International Geology Review 49, 193-234.

Cameron, A.E., Smith, D.H., Walker, R.L. 1969. Mass spectrometry of nanogram-size samples of lead. Analytical Chemistry 41, 525-526.

Carroll, M. R., Wyllie, P. J. 1990. The system tonalite-H_2O at 15 kbar and the genesis of calc-alkaline magmas. American Mineralogist 75, 345–357.

Chappell, B. W., White, A. J. R. 2001. Two contrasting granite types: 25 years later. Australian Journal of Earth Sciences 48, 489-499.

Clemens, J. D., Stevens, G. 2012. What controls chemical variation in granitic magmas? Lithos, 134-135, 317-329.

Clemens, J.D., Stevens, G., Farina, F., 2011. The enigmatic sources of I-type granites: The peritectic connexion. Lithos 126, 174-181.

Coleman, D. S., Glazner, A. F. 1997. The sierra crest magmatic event: rapid formation of juvenile crust during the late cretaceous in California. International Geological Review 39, 768-787.

Coleman, D. S., Glazner, A. F., Frost, T. P. 1992. Evidence from the Lamarck granodiorite for rapid late cretaceous crust formation in California. Science 258, 1924-1926.

Coleman, D. S., Glazner, A. F., Miller, J. S., Bradford, K. J., Frost, T. P., Joye, J. L., Bachl, C. A. 1995. Exposure of a late Cretaceous layered mafic felsic magma system in the central Sierra Nevada batholith, California. Contributions to Mineralogy and Petrology 120, 129-136.

DePaolo, D. J. 1981. Trace element and isotopic effects of combined wall rock assimilation and fractional crystallization. Earth and Planetary Science Letters 53, 189-202.

DePaolo, D. J. 1981. A neodymium and strontium isotopic study of the Mesozoic Calc-Alkaline Granitic Batholiths of the Sierra Nevada and peninsular ranges, California. Journal of Geophysical Research 86, 10470-10488.

Dorais, M. J., Whitney, J. A., Roden, M. F. 1990. Origin of mafic enclaves in the Dinkey Creek Pluton, Central Sierra Nevada Batholith, California. Journal of Petrology 31, 853-881.

Dufek, J., Bergantz, G.W. 2005. Lower crustal magma genesis and preservation: a stochastic framework for the evaluation of basalt-crust interaction. Journal of Petrology 46, 2167-2195.

Frost, T. P., Mahood, G. A. 1987. Field, chemical, and physical constraints on mafic-felsic magma interaction in the Lamarck Granodiorite, Sierra Nevada, California. Geological Society America Bulletin 99, 272-291.

Frost, B.R., Barnes, C. G.,Collins, W. J., Arculus, R. J., Ellis, D. J., Frost, C.D. 2001. A geochemical classification for granitic rocks. Journal of Petrology 42, 2033-2048.

Frost, B.R., Frost, C.D. 2008. A geochemical classification for feldspathic rocks. Journal of Petrology 49, 1955-1969.

Gill, J. 1981. Orogenic Andesites and Plate Tectonics. Berlin: Springer, 390 p.

Gerstenberger, H., Haase, G. 1997. A highly effective emitter substance for mass spectrometric Pb isotope ratio determinations. Chemical Geology 136, 309-312

Green, R.W.E., 1983. Seismic refraction observations in the Damara orogen and flanking craton and their bearing on deep seated processes in the orogen. Special Publication Geological Society of South Africa 11, 355– 367.

Green, D. H., Hibberson, W. O., Kovacs, I., Rosenthal, A. 2010. Water and its influence on the lithosphere/asthenosphere boundary. Nature 467, 448-451.

Grove,T. L., Kinzler, R. J. 1986. Petrogenesis of Andesites. Annual Review of Earth and Planetary Sciences 14, 417-454.

Grove, T. L., Kinzler, R. J., Baker, M. B., Donnelly-Nolan, J. M., Lesher, C. E. 1988. Assimilation Of Granite by Basaltic Magma at Burnt Lava Flow, Medicine Lake Volcano, Northern California - Decoupling of Heat And Mass Transfer. Contributions to Mineralogy and Petrology 99, 320-343.

Grove, T. L., Donnelly-Nolan, J. M., Housh, T. 1997. Magmatic processes that generated the rhyolite of Glass Mountain, Medicine Lake volcano, N California. Contributions to Mineralogy and Petrology 127, 205-223.

Haack, U., Hoefs, J., Gohn, E., 1982. Constraints on the origin of Damaran granites by Rb/Sr and $\delta^{18}O$ data. Contributions to Mineralogy and Petrology 79, 279-289.

Harley, S. L. 1998. On the occurrence and characterization of ultrahigh-temperature crustal metamorphism. In: Treloar, P. J. and O'Brien, P. J. (eds) What drives metamorphism and metamorphic relations? Geological Society, London, Special Publications 138, 81-107.

Hartmann, O., Hoffer, E., Haack, U. 1983. Regional metamorphism in the Damara orogen: interaction of crustal motion and heat transfer. Special Publication Geological Society South Africa, 11, 233-241.

Harrison, T. M., Watson, E. B. 1984. The behaviour of apatite during crustal anatexis:

equilibrium and kinetic considerations. Geochimica et Cosmochimica Acta 48,1467-1477.

Hawkesworth, C. J., Menzies, M. A., van Calsteren, P. 1986. Geochemical and tectonic evolution of the Damara belt. In. Coward, M. P., Ries, A. C. (eds). Collision tectonics. Geological Society Special Publication 19, 305-319.

Heinrichs, H., Hermann, A.G., 1990. Praktikum der analytischen Geochemie. Springer Verlag, Berlin. 669 pp.

Helz, R., 1976. Phase relations of basalt in their melting ranges at P H_2O=5 kb: Part 2. Melt compositions. Journal of Petrology 17, 139-193.

Hildreth, W., Moorbath, S. 1988. Crustal contributions to arc magmatism in the Andes of Central Chile. Contributions to Mineralogy and Petrology 98, 455-489.

Hoernes, S., Hoffer, E. 1979. Equilibrium relations of prograde metamorphic mineral assemblages - a stable isotope study of rocks of the Damara orogen. Contributions to Mineralogy and Petrology 68, 377-389.

Holden, P., Halliday, A. N., Stephens, W. E. 1987. Neodymium and strontium isotope content of microdiorite enclaves points to mantle input to granitoid production. Nature, 330, 53–56

Huang, W. L., Wyllie, P. J. 1986. Phase relationships of gabbro-tonalite-granite-water at 15 kbar with applications to differentiation and antexis. American Mineralaogist 71, 301-316.

Jacobsen, S.B., Wasserburg, G.J., 1980. Sm-Nd isotopic evolution of chondrites. Earth and Planetary Science Letters 50, 139-155.

Jung, C., Jung, S., Nebel, O., Hellebrand, E., Masberg, P., Hoffer, E. 2009. Fluid-present melting of meta-igneous rocks and the generation of leucogranites – Constraints from garnet major- and trace element data, Lu-Hf whole rock-garnet ages and whole rock Nd-Sr-Hf-O isotope data. Lithos 111, 220-235.

Jung, S. 2005. Isotopic equilibrium/disequilibrium in granites, metasedimentary rocks and migmatites (Damara orogen, Namibia) – a consequence of polymetamorphism and melting. Lithos 84, 168-184.

Jung, S. 2000. High-temperature, mid-pressure clockwise P-T paths and melting in the development of regional migmatites: The role of crustal thickening and repeated plutonism. Geological Journal 35, 345-359.

Jung, S., Hellebrand, E. 2006. Trace element fractionation during high-grade metamorphism and crustal melting-constraints from ion microprobe data of metapelitic, migmatitic and igneous garnets and implications for Sm-Nd garnet chronology. Lithos 87, 193-213.

Jung, S., Hellebrand, E. 2007. Textural, geochronological and chemical constraints from polygenetic titanite and monogenetic apatite from a mid-crustal shear zone: an integrated EPMA, SIMS, and TIMS study. Chemical Geology 241, 88-107.

Jung, S., Mezger, K., 2001. Geochronology in migmatites; a Sm–Nd, U–Pb and Rb–Sr study from the Proterozoic Damara Belt (Namibia); implications for polyphase development of migmatites in high-grade terranes. Journal of metamorphic Geology 19, 77-97.

Jung, S., Mezger, K. 2003. Petrology of basement-dominated terranes: I. Regionalmetamorphic P-T-t path from U-Pb monazite and Sm-Nd garnet geochronology (Central Damara orogen, Namibia). Chemical Geology 198, 223-247.

Jung, S., Mezger, K., Hoernes, S., 1998. Petrology and geochemistry of syn- to post-collisional metaluminous A-type granites - a major and trace element and Nd–Sr–Pb–O study from the Proterozoic Damara Belt, Namibia. Lithos 45, 147– 175.

Jung, S., Hoernes, S., Mezger, K., 2000. Geochronology and petrogenesis of Pan-African, syn-tectonic, S-type and post-tectonic A-type granite (Namibia): products of melting of crustal sources, fractional crystallization and wall rock entrainment. Lithos 50, 259–287.

Jung, S., Hoernes, S., Mezger, K., 2001. Trace element and isotopic (Sr, Nd, Pb, O) arguments for a mid crustal origin of Pan-African garnet-bearing S-type granites from the Damara orogen (Namibia). Precambrian Research 110, 325– 355.

Jung, S., Hoernes, S., Mezger, K., 2002. Synorogenic melting of mafic lower crust: constraints from geochronology, petrology and Sr, Nd and O isotope geochemistry of quartz diorites (Damara orogen, Namibia). Contribution to Mineralogy and Petrology 143, 551–566.

Jung, S., Mezger, K., Hoernes, S., 2003. Petrology of basement-dominated terranes: II. Contrasting isotopic (Sr, Nd, Pb and O) signatures of basement-derived granites and constraints on the source region of granite (Damara orogen, Namibia). Chemical Geology 199, 1-28.

Jung, S., Masberg, P., Mihm, D., Hoernes, S. 2009. Partial melting of diverse crustal sources — Constraints from Sr–Nd–O isotope compositions of quartz diorite–granodiorite–leucogranite associations (Kaoko Belt, Namibia). Lithos 111, 236–251.

Jung, S, Mezger, K., Nebel, O., Kooijman, E. Berndt, J., Hauff, F., Münker, C. 2012. Origin of Meso-Proterozoic post-collisional leucogranite suites (Kaokoveld, Namibia): constraints from geochronology and Nd, Sr, Hf and Pb isotopes. Contributions to Mineralogy and Petrology 163, 1-17.

Kelsey, D. E. 2008. On ultrahigh-temperature crustal metamorphism. Gondwana Research 13, 1-29.

Kistler, R. W., Chappell, B. W., Peck, D. L., Bateman, P. C. 1986. Isotopic variation in the Tuolumne Intrusive Suite, central Sierra Nevada, California. Contributions to Mineralogy and Petrology 94, 205-220.

Lechler, P. J., Desilets, M. O. 1987. A review of the use of loss on ignition as a measure of total volatiles in whole rock analyses. Chemical Geology 63, 341-344.

Masberg, H. P., Hoffer, E., Hoernes, S., 1992. Microfabrics indicating granulite-facies metamorphism in the low-pressure central Damara Orogen, Namibia. Precambrian Research 55, 243-257.

McDermott, F., Hawkesworth, C.J., 1990. Intracrustal recycling and upper-crustal evolution: A case study from the Pan-African Damara mobile belt, central Namibia. Chemical Geology 83, 263-280.

McDermott, F., Harris, N.B.W., Hawkesworth, C.J., 1996. Geochemical constraints on crustal anatexis: a case study from the Pan-African Damara granitoids of Namibia. Contributions to Mineralogy and Petrology 123, 406– 423.

McDermott, F., Harris, N.B.W., Hawkesworth, C.J. 2000. Geochemical constraints on the petrogenesis of Pan-African A-type granites in the Damara Belt, Namibia. Communications geological Survey Namibia 12, 139-148.

Michard, A., 1989. Rare-earth element systematics in hydrothermal fluids. Geochimica et Cosmochimica Acta 53, 745-750.

Miller, R. Mc. G. 1983. The Pan-African Damara Orogen of Namibia. In: Miller, R. Mc. G. (Ed.) The Damara Orogen. Special Publication Geologicl Society of South Africa 11, 431-515.

Miller, R. McG. 2008. The geology of Namibia. Vol 1-3. Ministry of Mines and Energy, Geological Survey, Windhoek.

Musselwhite, D. S., De Paolo, D. J., McCurry, M. 1989. The evolution of a silicic magma system: isotopic and chemical evidence from the Woods Mountains Volcanic Center, Eastern California. Contributions to Mineralogy and Petrology 101, 19-29.

Nelson, W. R., Dorais, M. J., Christiansen, E. H., Hart, G. L. 2013. Petrogenesis of Sierra Nevada plutons inferred from the Sr, Nd, and O isotopic signatures of mafic igneous complexes in Yosemite Valley, California. Contributions to Mineralogy and Petrology 165, 397-417.

Petford, N., Atherton, M., 1996. Na-rich partial melts from newly underplated basaltic crust: the Cordillera Blanca batholith, Peru. Journal of Petrology 37, 1491-1521.

Petford, N., Gallagher, K., 2001. Partial melting of mafic (amphibolitic) lower crust by periodic influx of basaltic magma. Earth and Planetary Science Letters 193, 483-499.

Puhan, D. 1983. Temperature and pressure of metamorphism in the Central Damara orogen. Special Publication Geological Society South Africa 11, 219-223.

Rapp, R. P., Watson, E. B., 1995. Dehydration melting of metabasalt at 8 – 32 kbar: implications for continental growth and crust – mantle recycling. Journal of Petrology 36, 891– 932.

Ratajeski, K., Glazner, A. F., Miller, B. V. 2001. Geology and geochemistry of mafic to felsic plutonic rocks in the cretaceous intrusive suite of Yosemite Valley, California. Geological Society America Bulletin 113, 1485-1602.

Ratajeski, K., Sisson, T. W., Glazner, A. F. 2005. Experimental and geochemical evidence for derivation of the El Capitan Granite, California, by partial melting of hydrous gabbroic lower crust. Contributions to Mineralogy and Petrology 149: 713-734.

Reid, J. B. Jr., Evans, O. C., Fates, D. G. 1983. Magma mixing in granitic rocks of the central Sierra Nevada, California. Earth and Planetary Science Letters 66, 243-261.

Reiners, P. W., Nelson, B. K., Ghiorso, M. S. 1995. Assimilation of felsic crust by basaltic magma: Thermal limits and extents of crustal contamination of mantle-derived magmas. Geology 23, 563-566

Roberts, M.P., Clemens, J.D. 1993. Origin of high-potassium, calc-alkaline, I-type granitoids. Geology 21, 825-828.

Rogers, G., Hawkesworth, C. J. 1989. A geochemical traverse across the North Chilean Andes - evidence for crust generation from the mantle wedge. Earth and Planetary Science Letters 91, 271–285.

Rollinson, H. R., 1993. Using geochemical data: evaluation, presentation, interpretation. Longman scientific and technical, 352 pp.

Rudnick, R. L., Fountain, D. M. 1995. Nature and composition of the continental crust: a lower crustal perspective. Reviews of Geophysics 33, 267–309.

Rutter, M.J., Wyllie, P.J. 1988. Melting of vapour-absent tonalite at 10 kbar to simulate dehydration-melting in the deep crust. Nature 331, 159-160.

Seth, B., Jung, S., Hoernes, S. 2002. Isotope constraints on the origin of Pan African granitoid rocks in the Kaoko Belt NW Namibia. South African Journal of Geology 105, 179-192.

Seth, B., Kröner, A., Mezger, K., Nemchin, A.A., Pidgeon, R.T., Okrusch, M. 1998. Archaean to Neoproterozoic magmatic events in the Kaoko belt of NW Namibia and their geodynamic significance. Precambrian Research 92, 341-363.

Sisson, T. W., Grove, T. L., Coleman, D. S. 1996. Hornblende gabbro sill complex at Onion Valley, California, and a mixing origin for the Sierra Nevada batholith. Contributions to Mineralogy and Petrology 126, 81-108.

Stacey, J.S., Kramers, J.D. 1975. Approximation of terrestrial lead isotope evolution by a two-stage model. Earth and Planetary Science Letters 26, 207-221.

Tepper, J.H., Nelson, B.K., Bergantz, G.W., Irving, A..J. 1993. Petrology of the Chilliwack batholith, North Cascades, Washington: generation of calc-alkaline granitoids by melting of mafic lower crust with variable water fugacity. Contributions to Mineralogy and Petrology 113, 333-351

Watson, E.B., Harrison, T.M., 1983. Zircon saturation revisited: temperature and composition effects in a variety of crustal magma types. Earth and Planetary Science Letters 64, 295-304.

Wenner, J. M., Coleman, D. S. 2004. Magma Mixing and cretaceous crustal growth: geology and geochemistry of granites in the Central Sierra Nevada Batholith, California. International Geological Review 46, 880-903.

Wolf, M. B., Wyllie, P. J., 1994. Dehydration-melting of amphibolite at 10 kbar: the effects of temperature and time. Contributions to Mineralogy and Petrology 115, 369–383.

Figure captions

Fig.1. Generalized geological map showing the study area within the Central Zone of the Damara orogen, Namibia. Abbreviations in inset: KZ: Kaoko Zone, NP: Northern Platform, NZ: Northern Zone, nCZ: northern central Zone, sCZ: southern Central Zone, SZ: Southern Zone, SMZ: Southern Margin Zone. Isograd map (Hartmann et al., 1983) gives the distribution of regional metamorphic isograds within the southern and central Damara orogen. Isograds: (1) biotite-in, (2) garnet-in, (3) staurolite-in, (4) kyanite-in, (5) cordierite-in, (6) andalusite <---> sillimanite, (7) sillimanite-in according to staurolite-breakdown, (8) partial melting due to: muscovite + plagioclase + quartz + H_2O <---> melt + sillimanite, (9) K-feldspar + cordierite-in, (10) partial melting due to: biotite + K-feldspar + plagioclase + quartz + cordierite <---> melt + garnet. W: Walvisbay, S: Swakopmund, Wh: Windhoek.

Fig. 2. Geological sketch map of the Gawib area and surroundings. Note the occurrence of the Palmental complex and other quartz diorite intrusions of the same age (Goas and Okongava; Jung et al., 2002) and the vicinity of numerous basement complexes and the Okahandja lineament (OL).

Fig. 3. U/Pb concordia diagram showing U-Pb zircon analyses from granodiorites (Gawib pluton).

Fig. 4. Major element plots for granodiorites and granites. Grey circles are analyses from Goas-Okongava (Jung et al., 2002) and Palmental (Jung et al. unpubl.). Fields for analyses from the Sierra Nevada batholith are indicated. For locations see Fig. 2.

Fig. 5. Selected trace element plots for granodiorites and granites. Grey circles are analyses from Goas-Okongava (Jung et al., 2002) and Palmental (Jung et al. unpubl.). Fields for analyses from the Sierra Nevada batholith are indicated. For locations see Fig. 2.

Fig. 6. Chondrite-normalized rare earth element plots for granodiorites and granites. Normalization factors according to Boynton (1984). Indicated are representative samples with lowest and highest REE abundances from each rock type. A field for analyses from the Sierra Nevada batholith is indicated.

Fig. 7. Initial εNd vs. initial $^{87}Sr/^{86}Sr$ diagram for granodiorites and granites. Grey circles are analyses from Goas-Okongava (Jung et al., 2002) and Palmental (Jung et al. unpubl.). For locations see Fig. 2. Field for mafic rocks from the Sierra Nevada Batholith is from Wenner and Coleman (2004), Nelson et al. (2013) and references therein.

Fig. 8. Plot of (a) $^{207}Pb/^{204}Pb$ and (b) $^{208}Pb/^{204}Pb$ vs $^{206}Pb/^{204}Pb$ isotope ratios of leached K-feldspar from granodiorites and granites. The curve represents the average Pb growth curve according to Stacey and Kramers (1975). Tick marks represent 250 Ma intervals. Grey circles are analyses from Goas-Okongava (Jung et al., 2002) and Palmental (Jung et al. unpubl.). For locations see Fig. 2. Analyses of metasedimentary rocks are form McDermott and Hawkesworth (1990).

Fig. 9 (a). Plot of Eu/Eu* (as a measure of the negative Eu anomaly) vs. Sr concentrations. (b) Rb-Sr variation among the granodiorites and granites to show effects of fractional crystallization processes. Mineral vectors calculated according to partition coefficients compiled in Rollinson (1993). For discussion see text.

Fig. 10. Plot of MgO vs. $^{206}Pb/^{204}Pb$ and initial εNd vs. $^{206}Pb/^{204}Pb$. Note a possible genetic relationship of the granodiorites to unexposed quartz diorites similar to the Palmental quartz diorites. For locations see Fig. 2.

Fig. 11. Plot of $^{87}Sr/^{86}Sr$ vs. ε Nd for granodiorites and granites and a possible calculated AFC curve. This calculation uses a hypothetical basement rock with 200 ppm Sr ($^{87}Sr/^{86}Sr$: 0.74) and 25 ppm Nd (ε Nd: -30). The starting granodiorite has 900 ppm Sr ($^{87}Sr/^{86}Sr$: 0.7068) and 50 ppm Nd (ε Nd: -6.5) similar to the most primitive granodiorite samples. Bulk K_D´s (Sr) and (Nd) were 0.5 with a r-value (ratio of assimilation to fractionation) of 0.6. The field of Kaokoveld gneisses is compiled from data of Seth et al. (2002) and the field of basement-derived granites from the Damara orogen is from Jung et al. (2003). Data for metasedimentary rocks are from McDermott and Hawkesworth (1990). Grey circles are analyses from Goas-Okongava (Jung et al., 2002) and Palmental (Jung et al. unpubl.). For locations see Fig. 2.

Fig. 12. ε Nd (inital) vs. $^{206}Pb/^{204}Pb$ for granodiorites and granites from the Gawib pluton. Also shown are analyses from other quartz diorites (Palmental, Goas-Okongava; Jung unpubl. And Jung et al., 2002) and a field for basement-derived granites from the Damara orogen (Jung et al., 2003). Note a possible genetic relationship of the granodiorites to unexposed quartz diorites similar to the Palmental quartz diorites. For further discussion see text.

Fig. 13. Primitive mantle-normalized multi element diagram showing the similarity between the Gawib granodiorite and arc-related intermediate magmas from the Sierra Nevada Batholith. Note the typical geochemical features such as negative anomalies in Nb, P and Ti (e.g. Nelson et al., 2013) and a positive Pb anomaly. For discussion see text.

Fig. 14. Plot of (a) TiO_2 vs. SiO_2 and (b) TiO_2 vs. temperature for granodiorites and experimental investigations. Note that the composition of the granodiorites is likely reproduced by high-

temperature melting of some sources reported by Rapp and Watson (1995). Grey circles in (a) are analyses from Goas-Okongava (Jung et al., 2002) and Palmental (Jung et al. unpubl.). For locations see Fig. 2. wm = wet melting, dm = dehydration melting.

Fig. 15. Plot of Fe+Mg+Ti values (in cation mole percentages) vs. experimental temperature using experiments of Rapp and Watson (1995). A possible melting temperature of c. 1040^{o}C (plus uncertainty) for the most primitive granodiorites from the Gawib pluton with Fe+Mg+Ti = 0.13 is indicated.

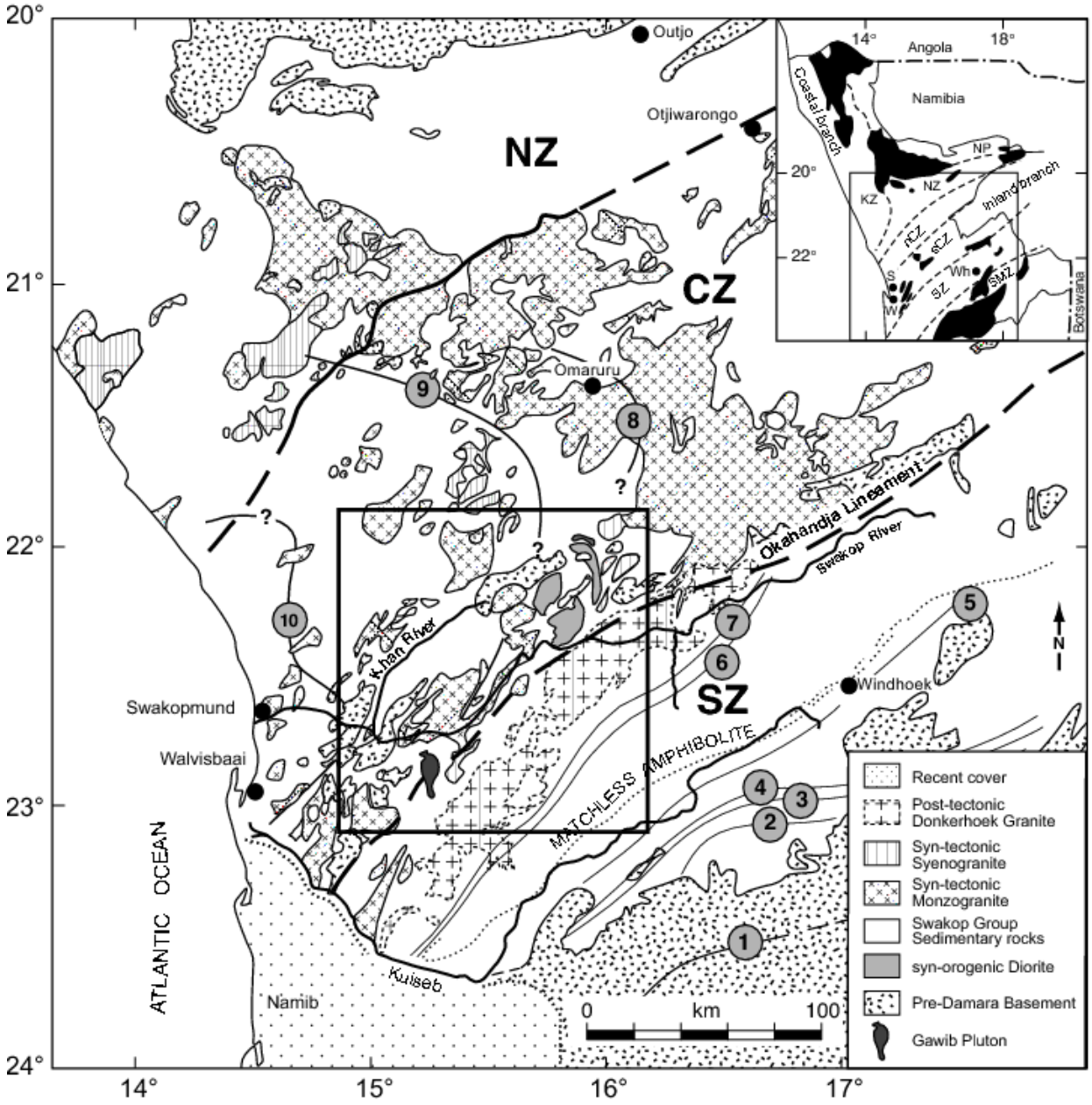

Fig. 1

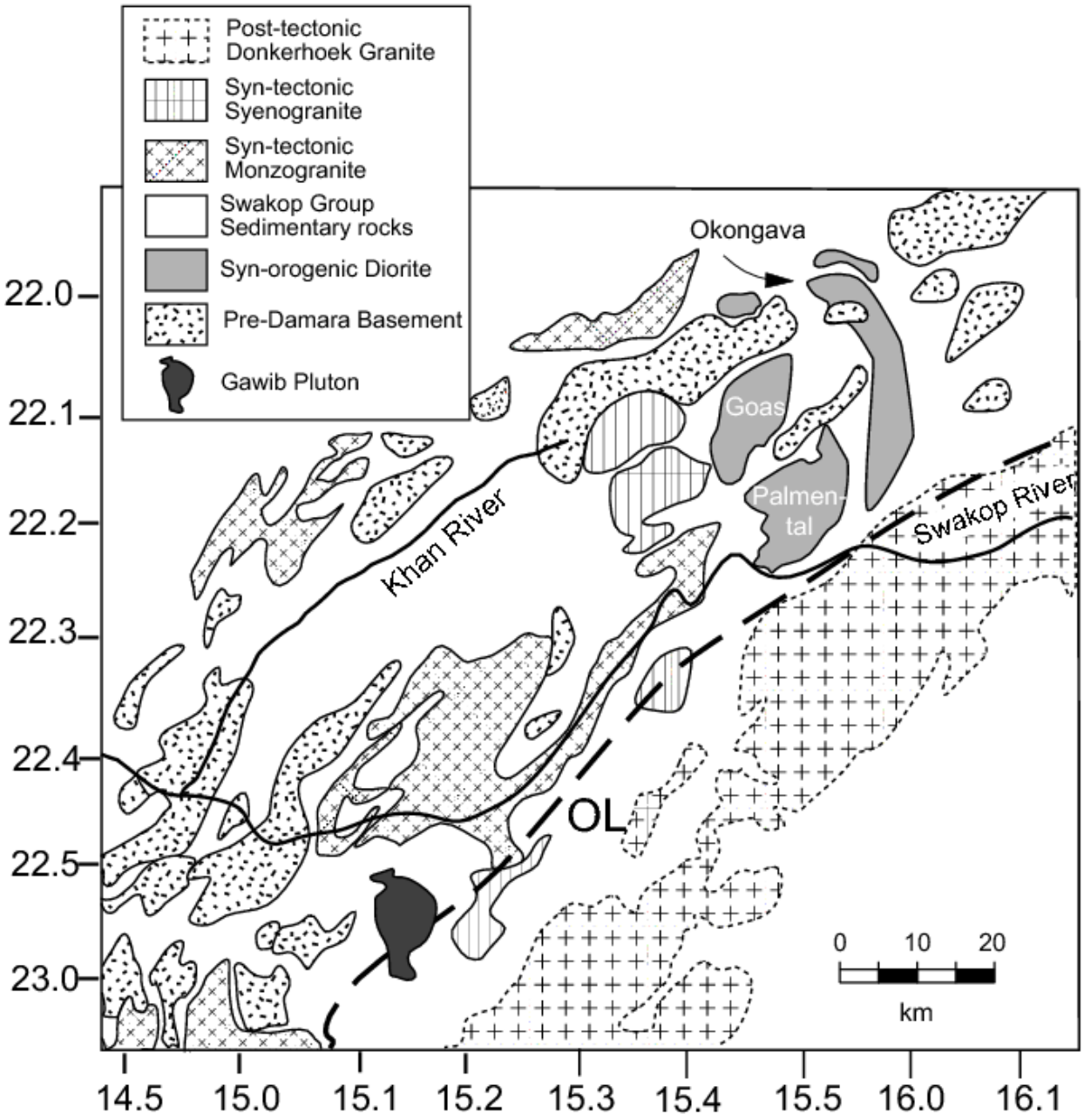

Fig. 2

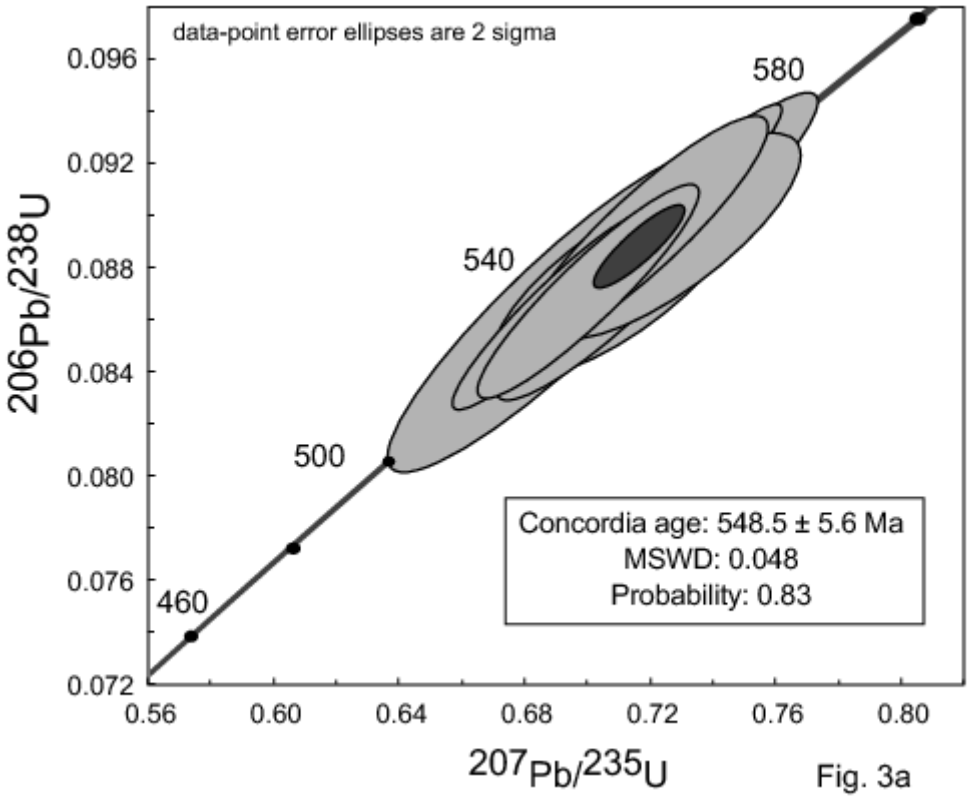

Fig. 3a

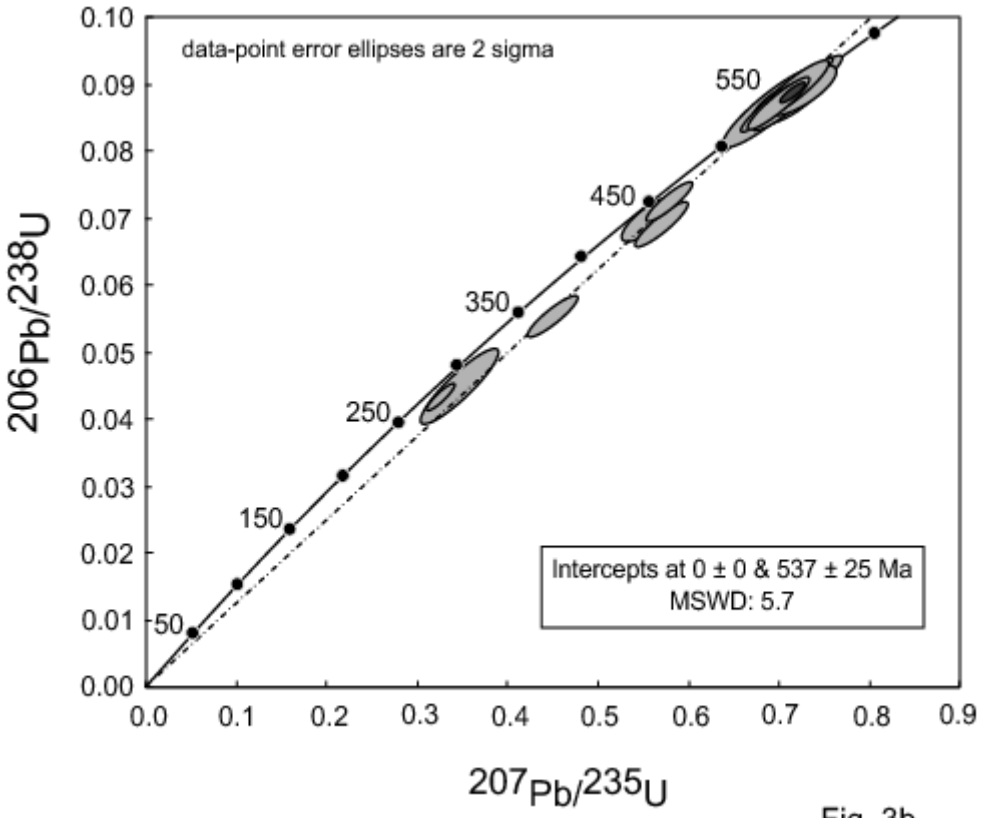

Fig. 3b

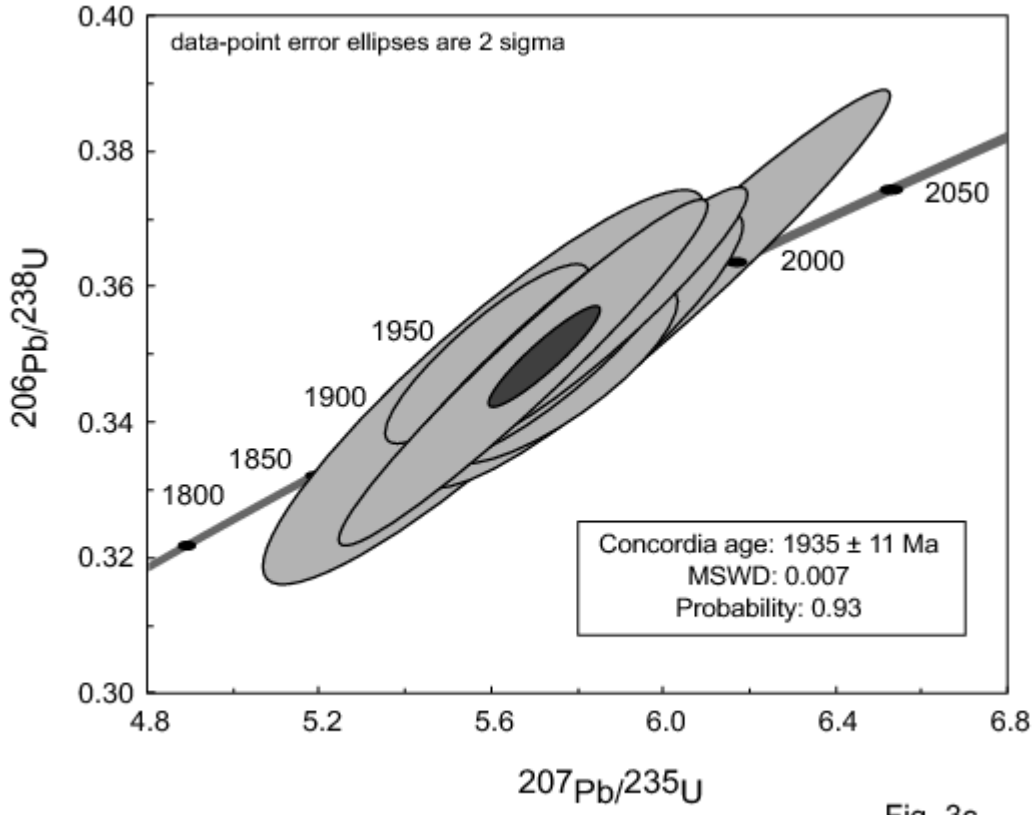

Fig. 3c

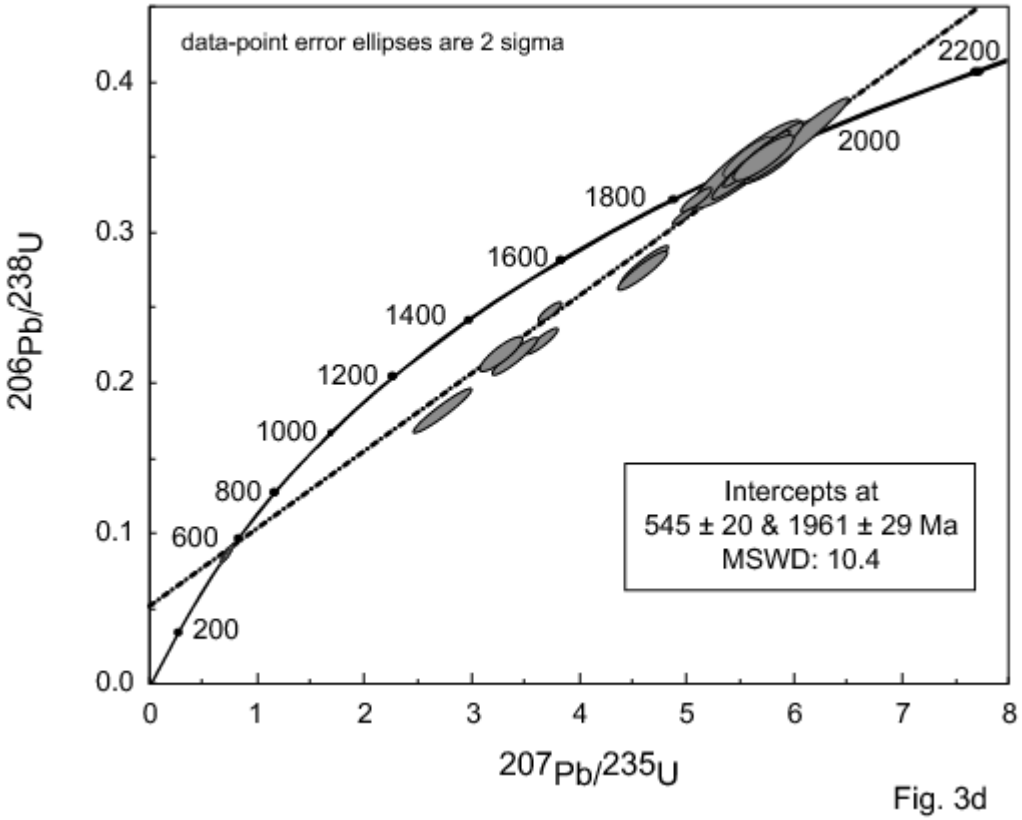

Fig. 3d

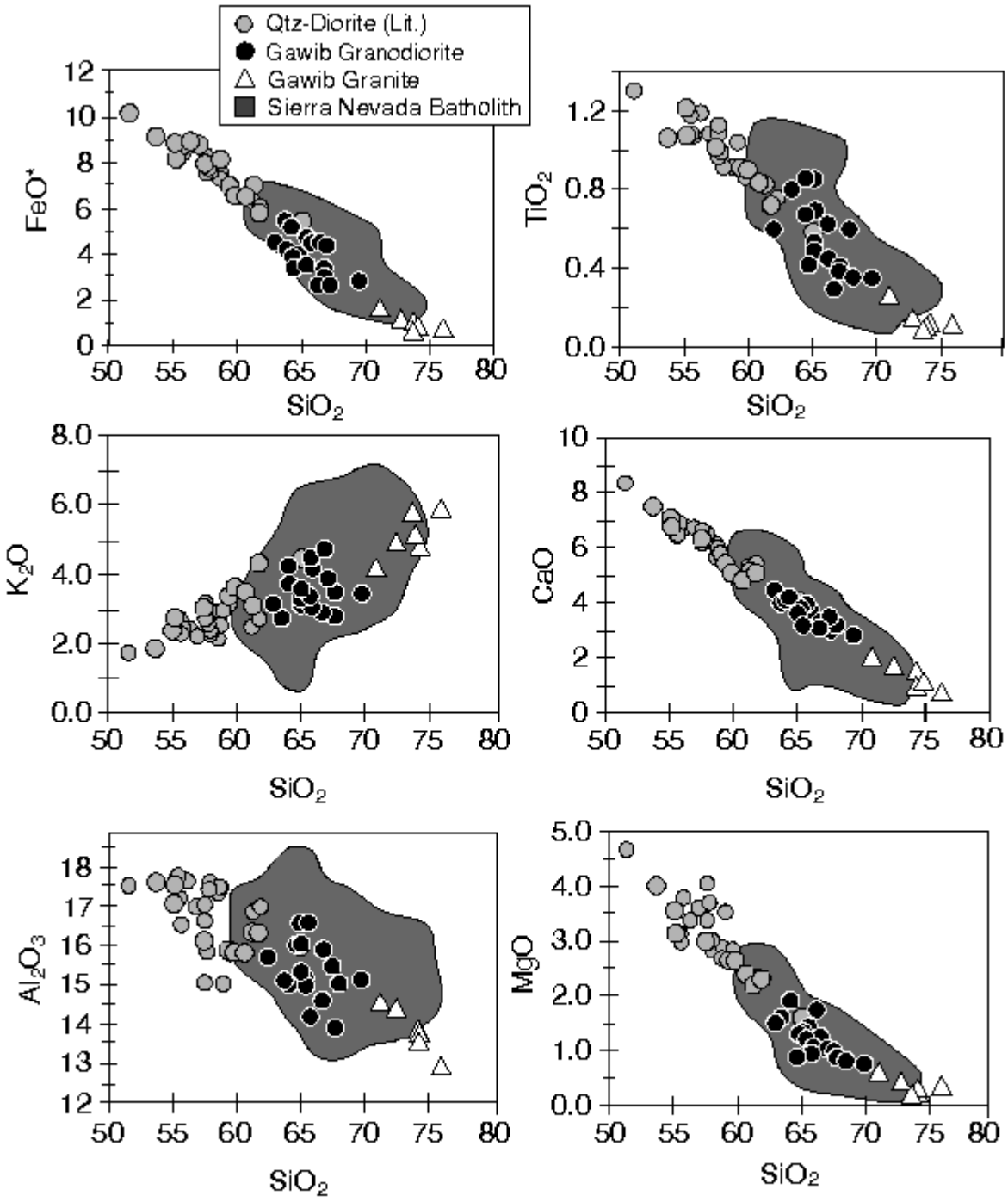

Fig. 4

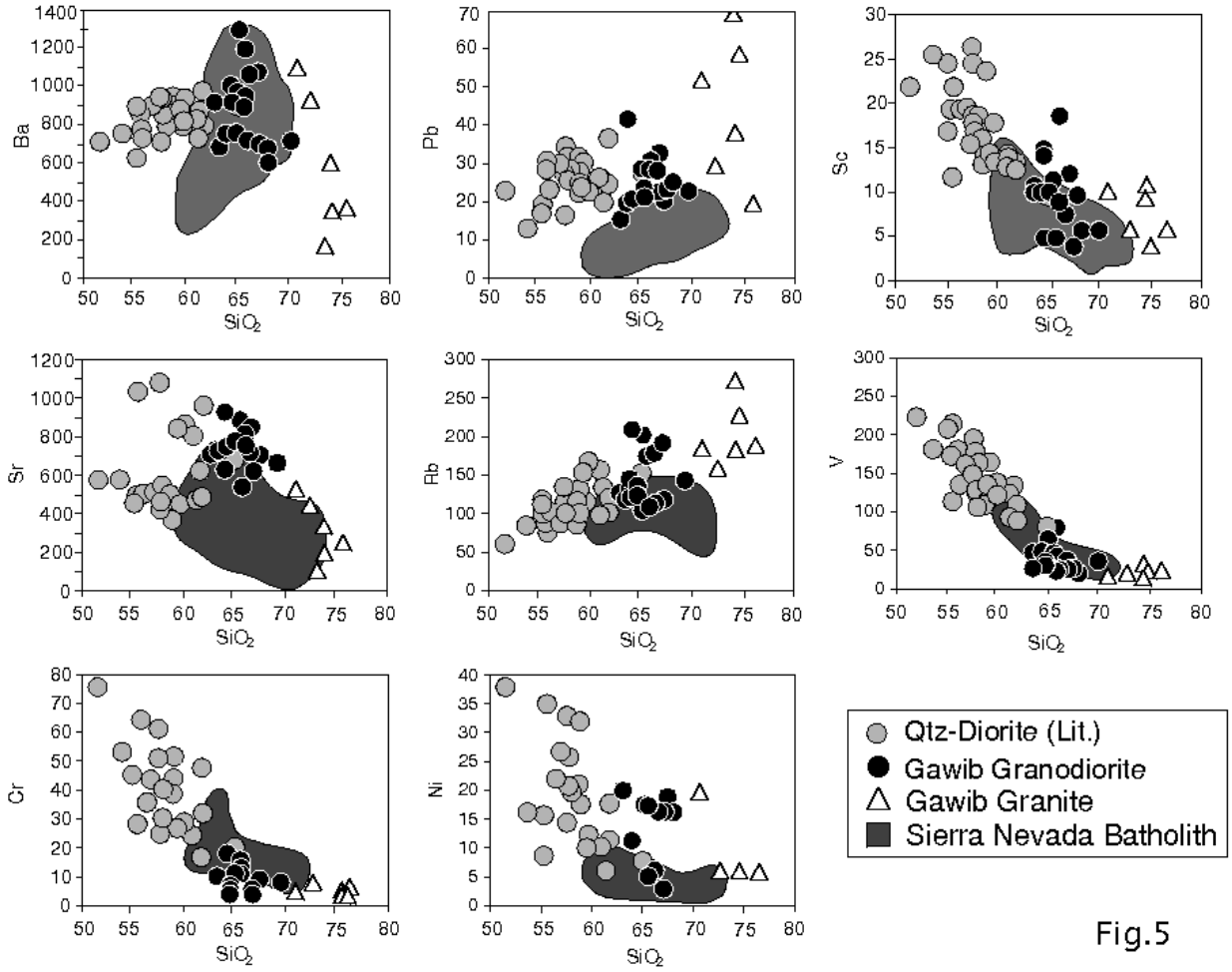

Fig.5

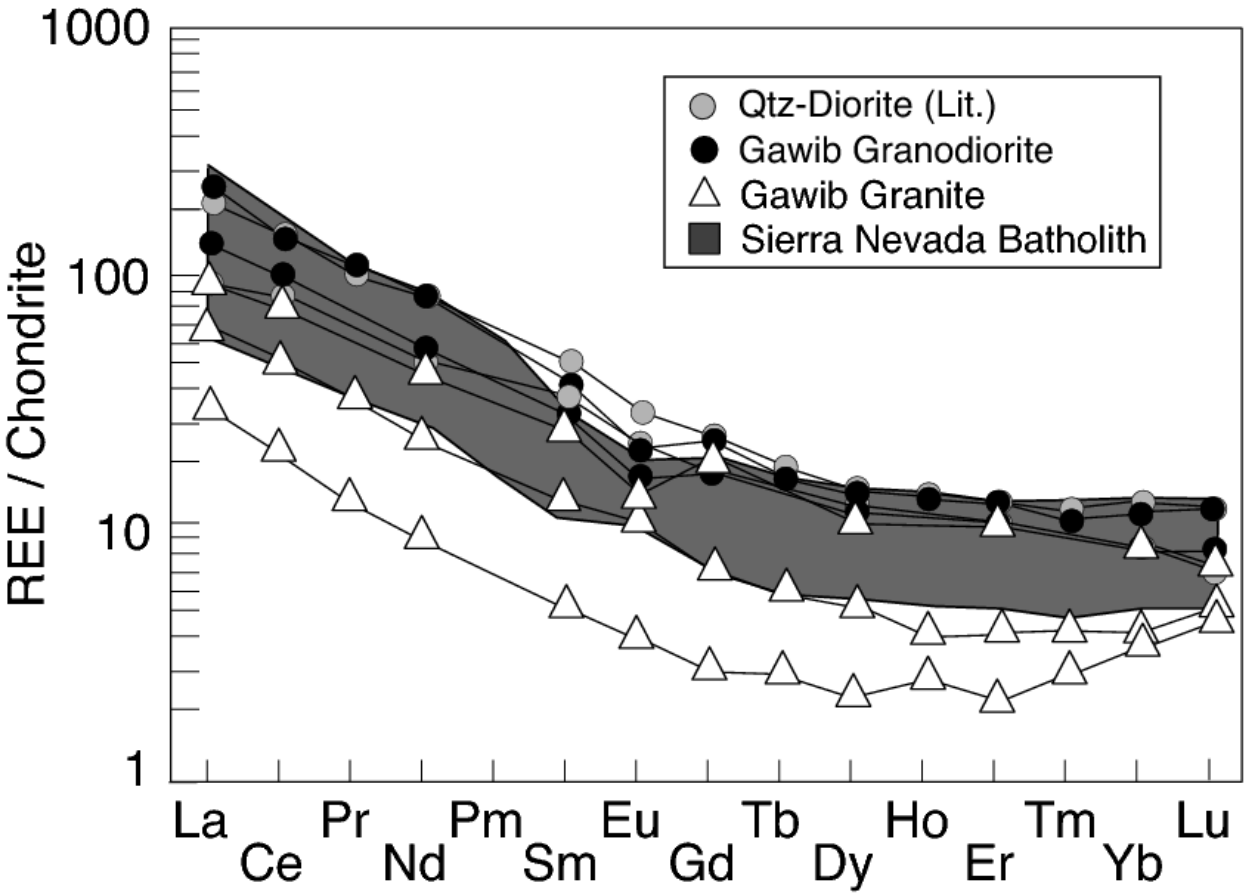

Fig. 6

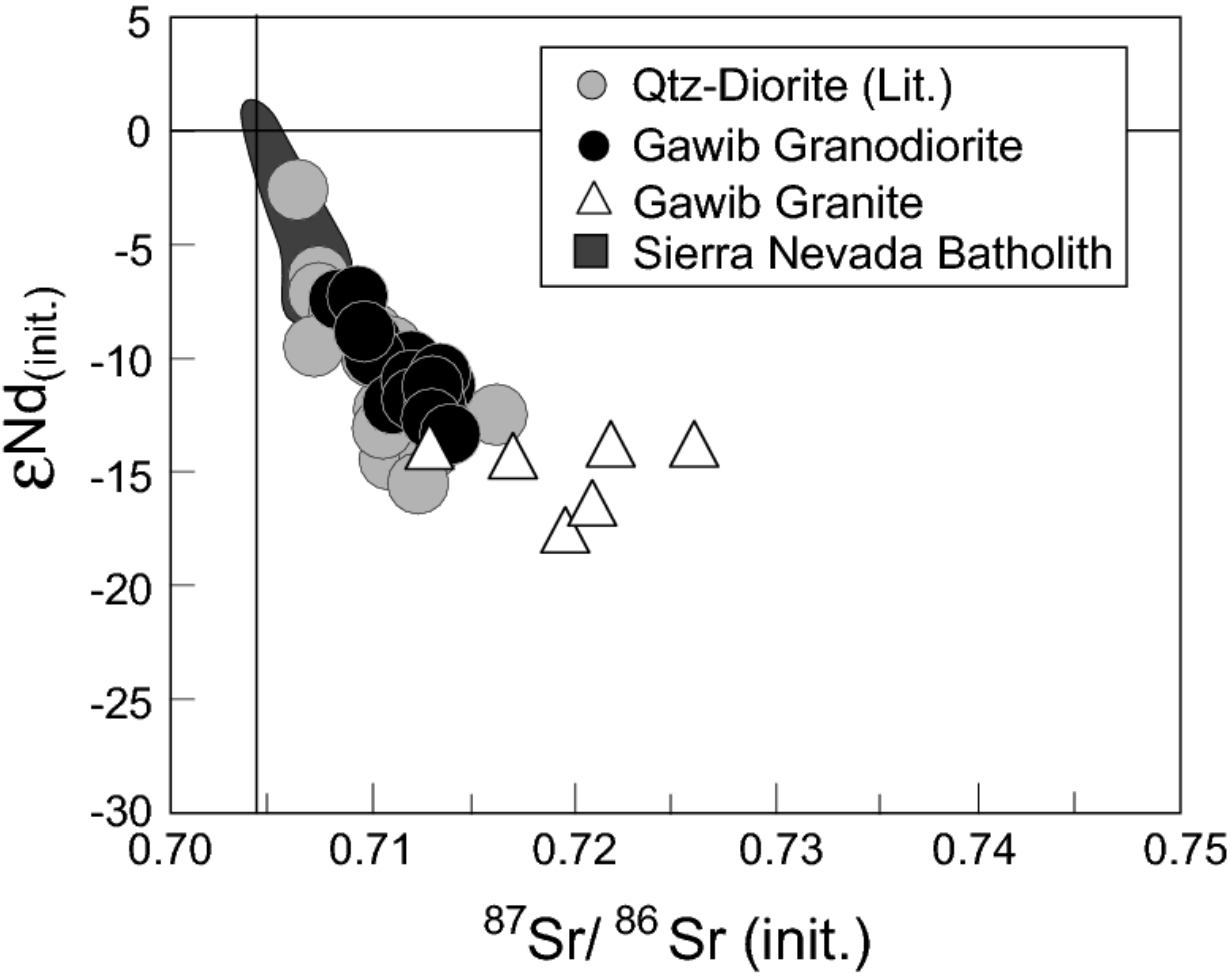

Fig. 7

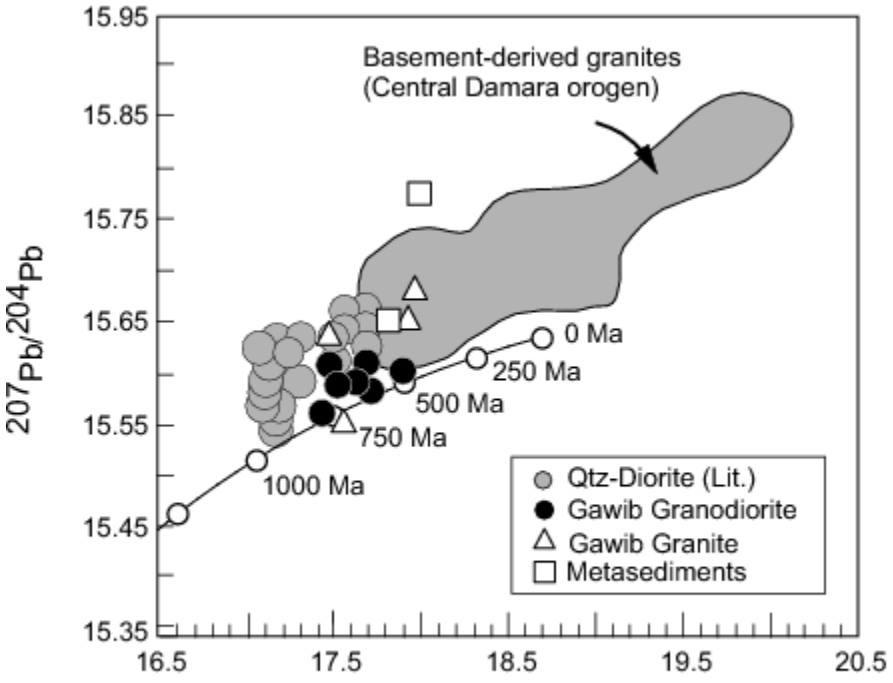

Fig. 8a

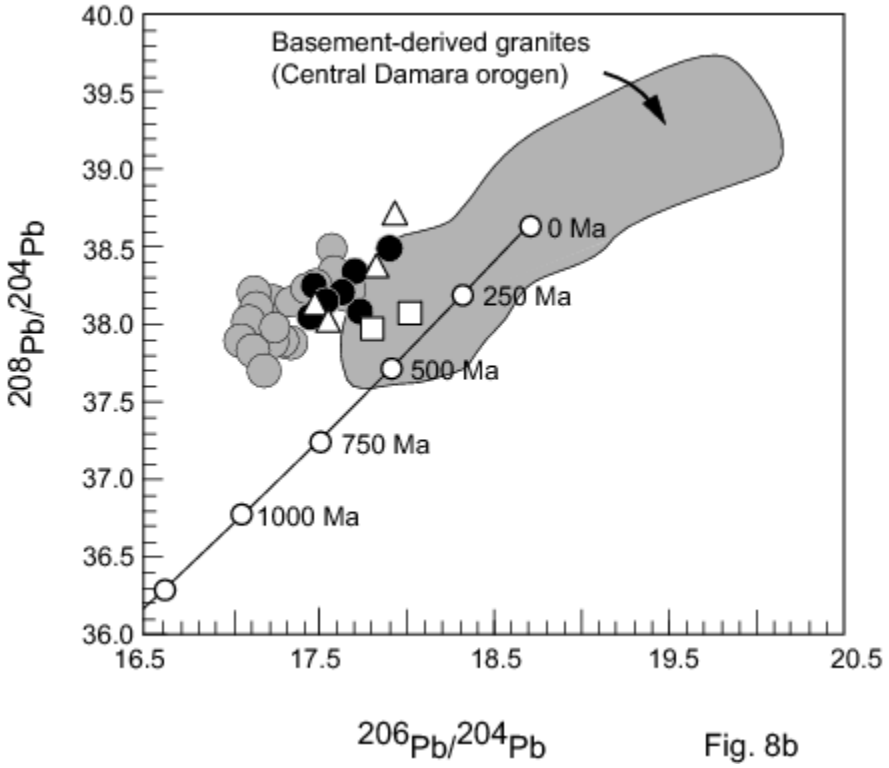

Fig. 8b

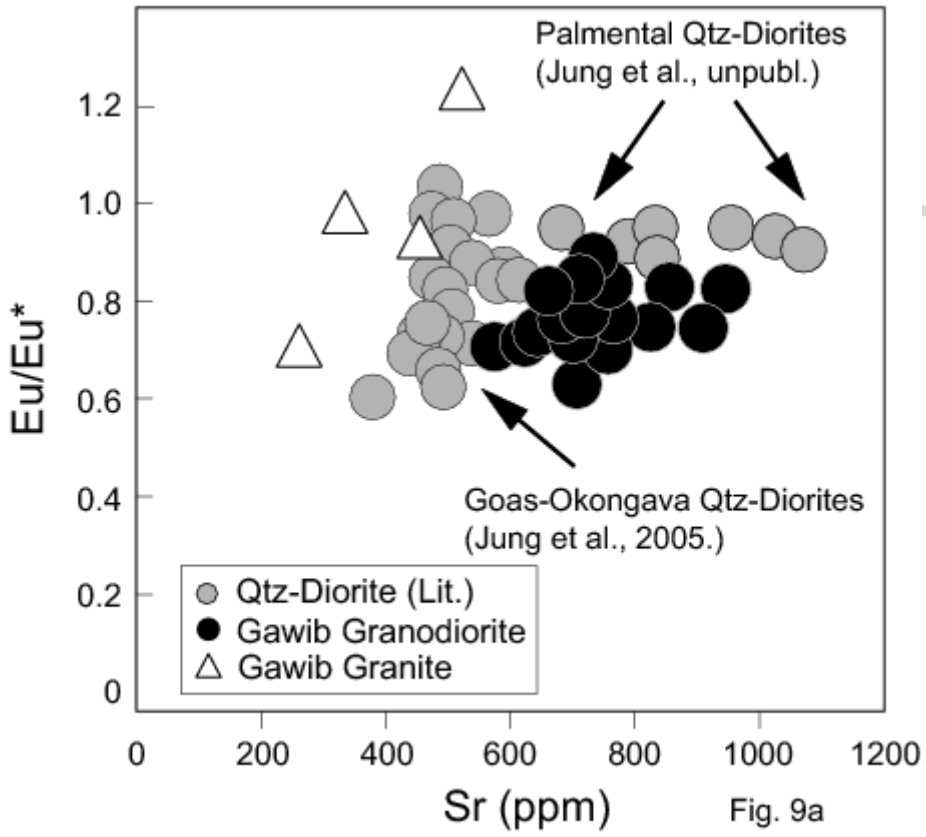

Fig. 9a

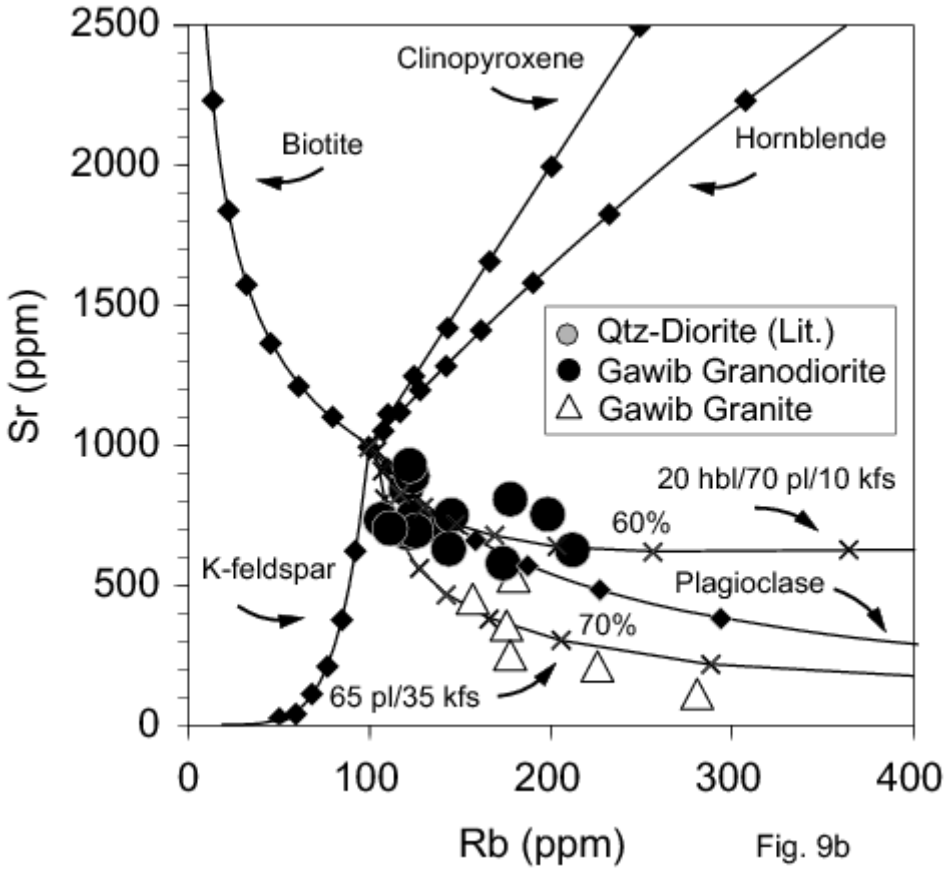

Fig. 9b

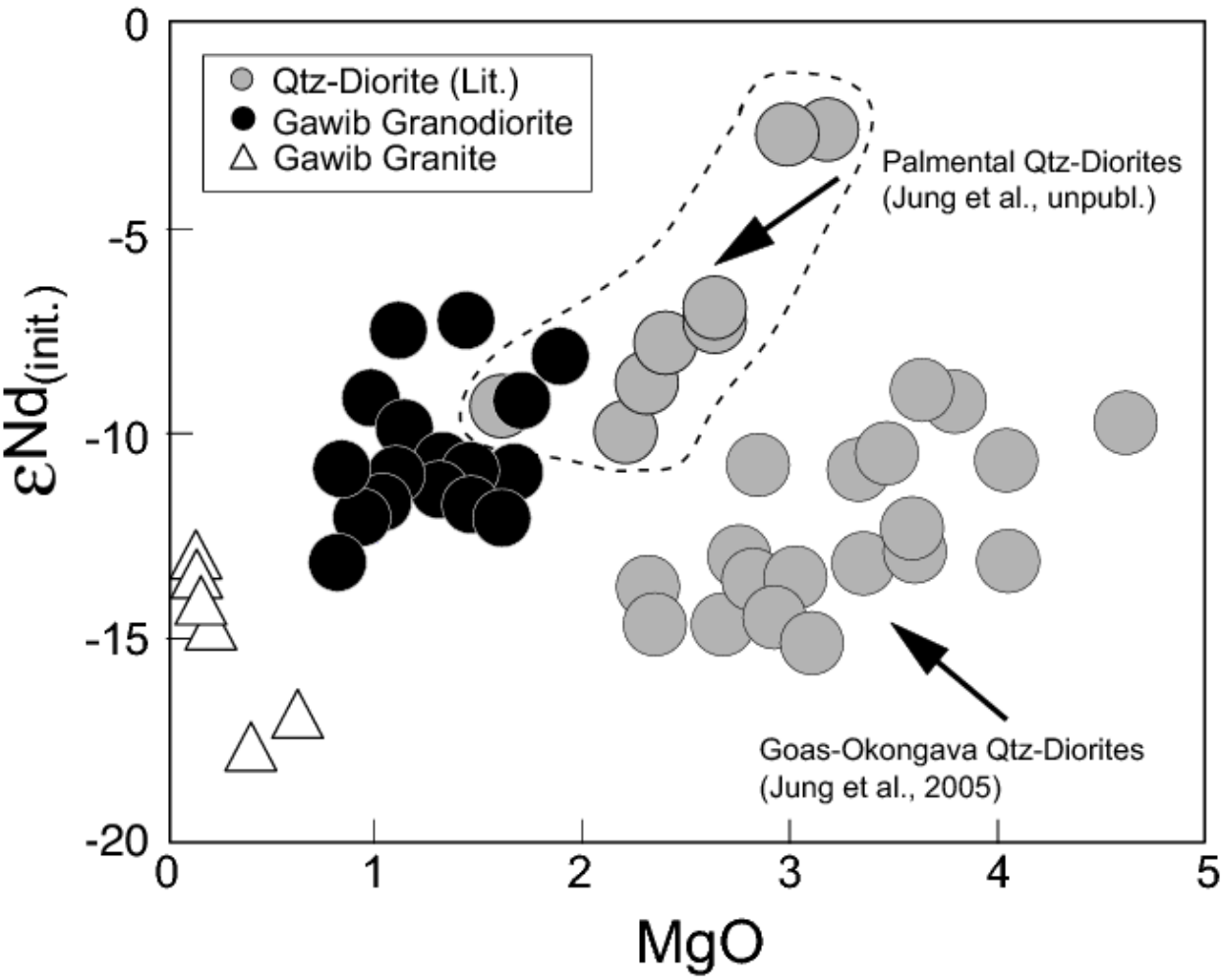

Fig. 10

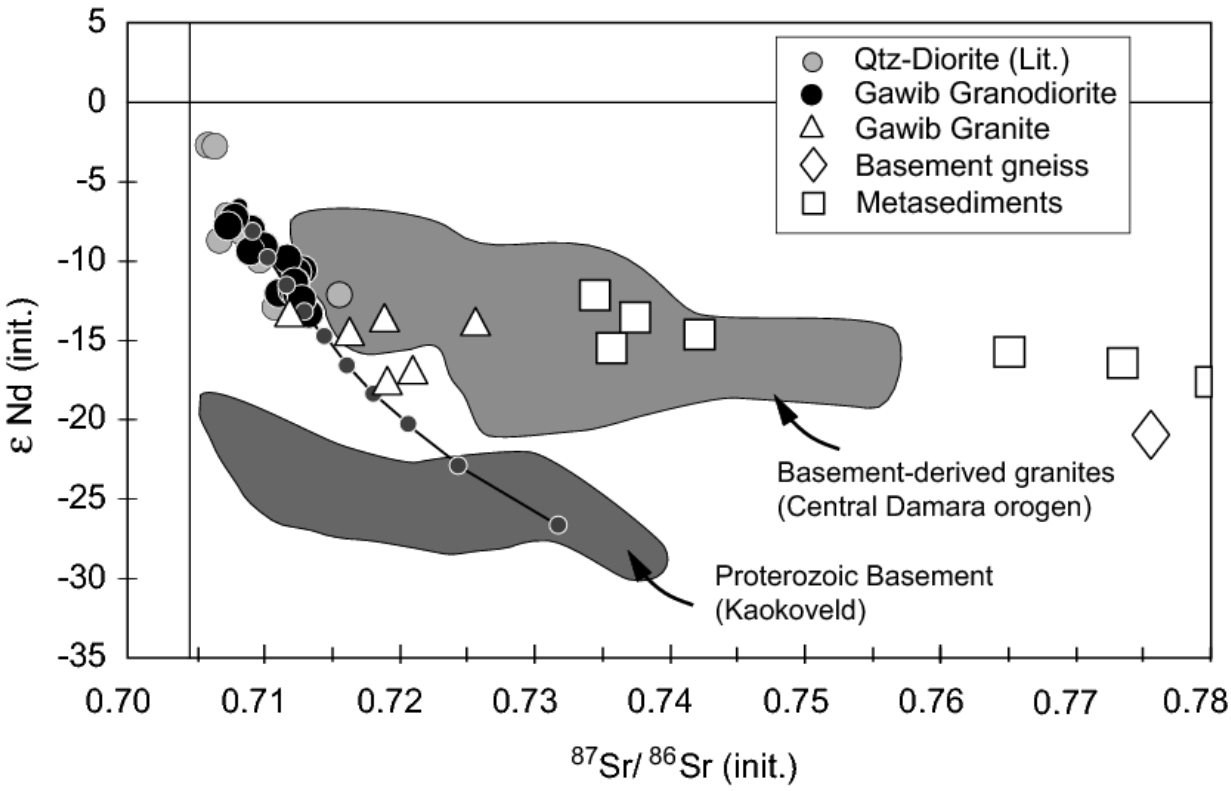

Fig. 11

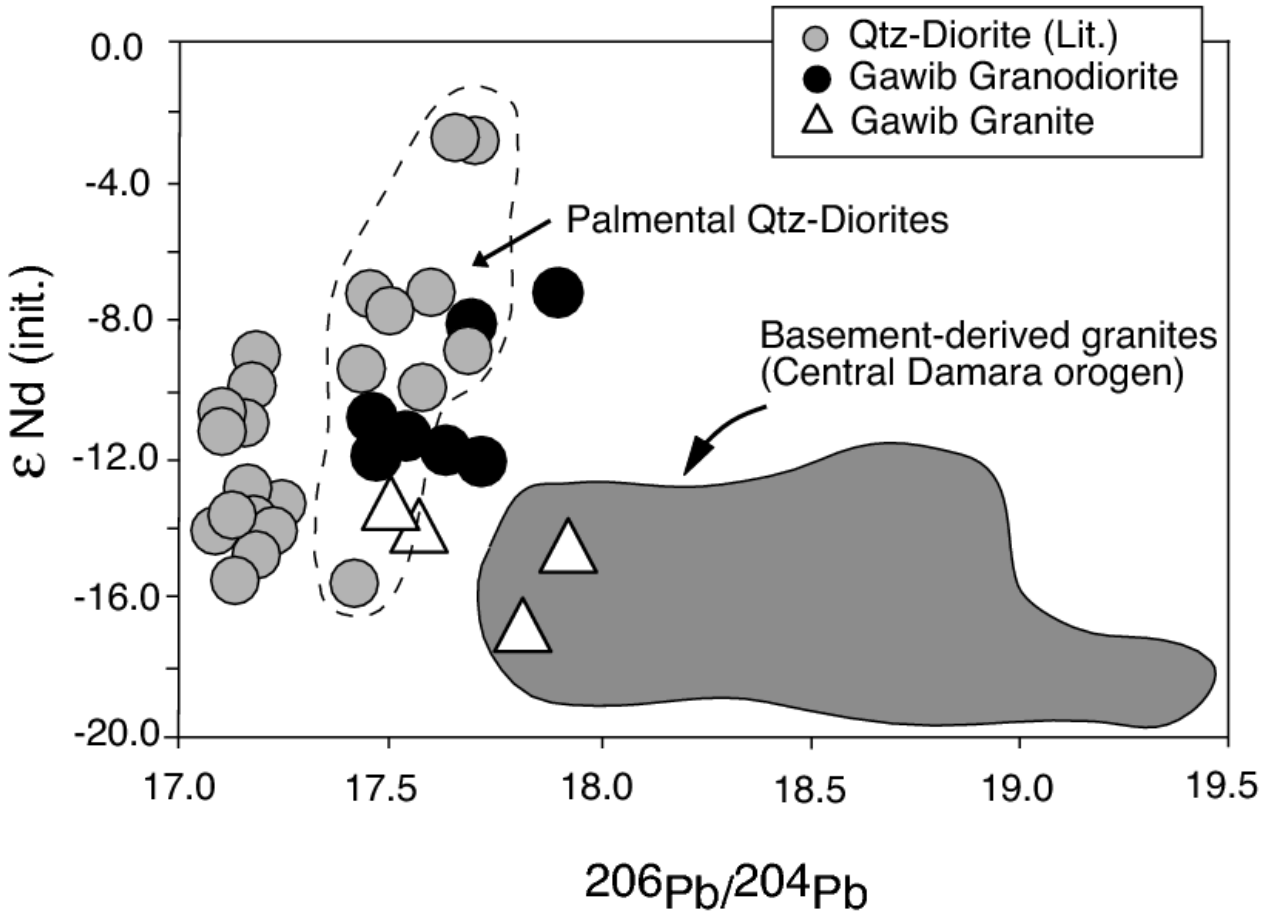

Fig. 12

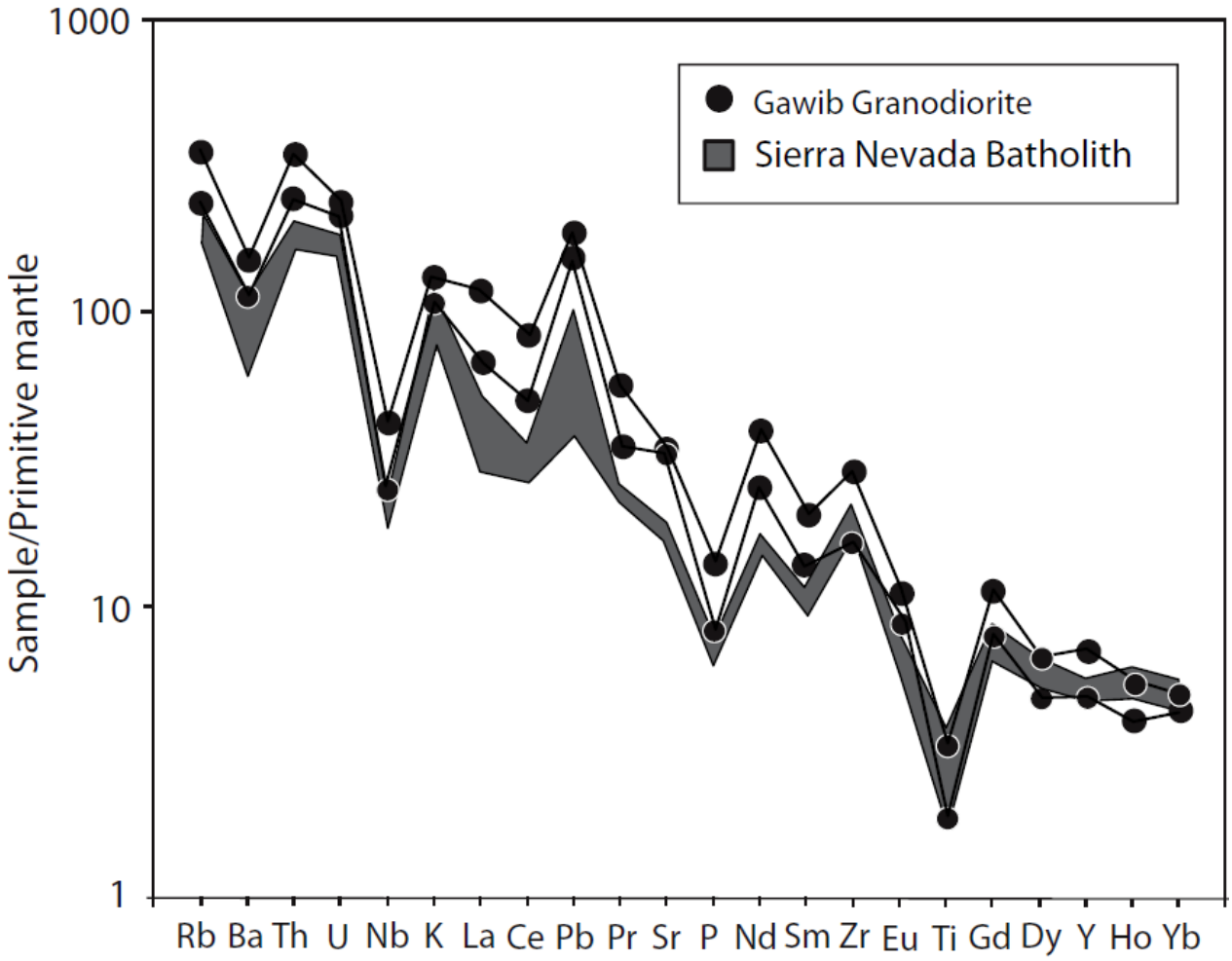

Fig. 13

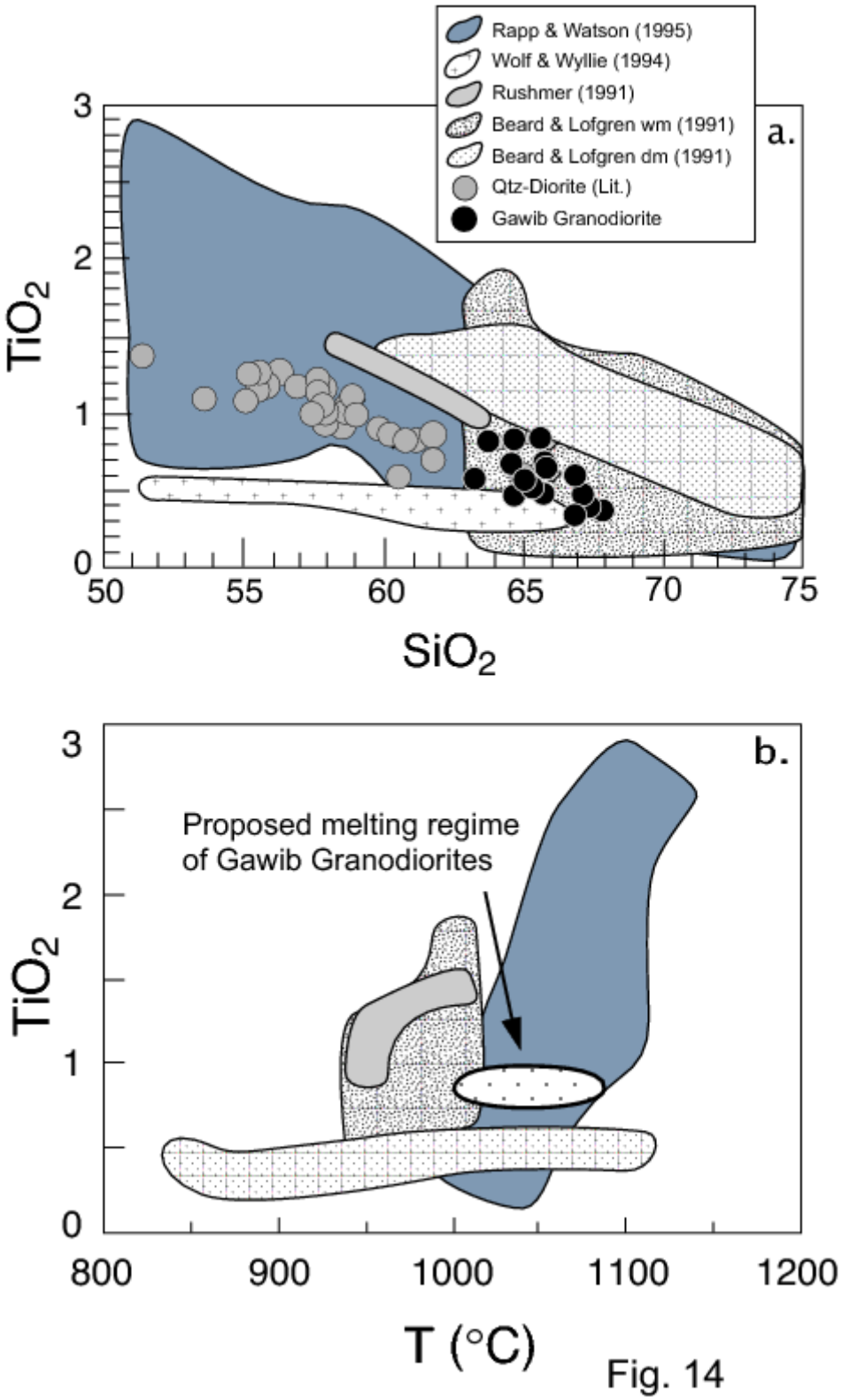

Fig. 14

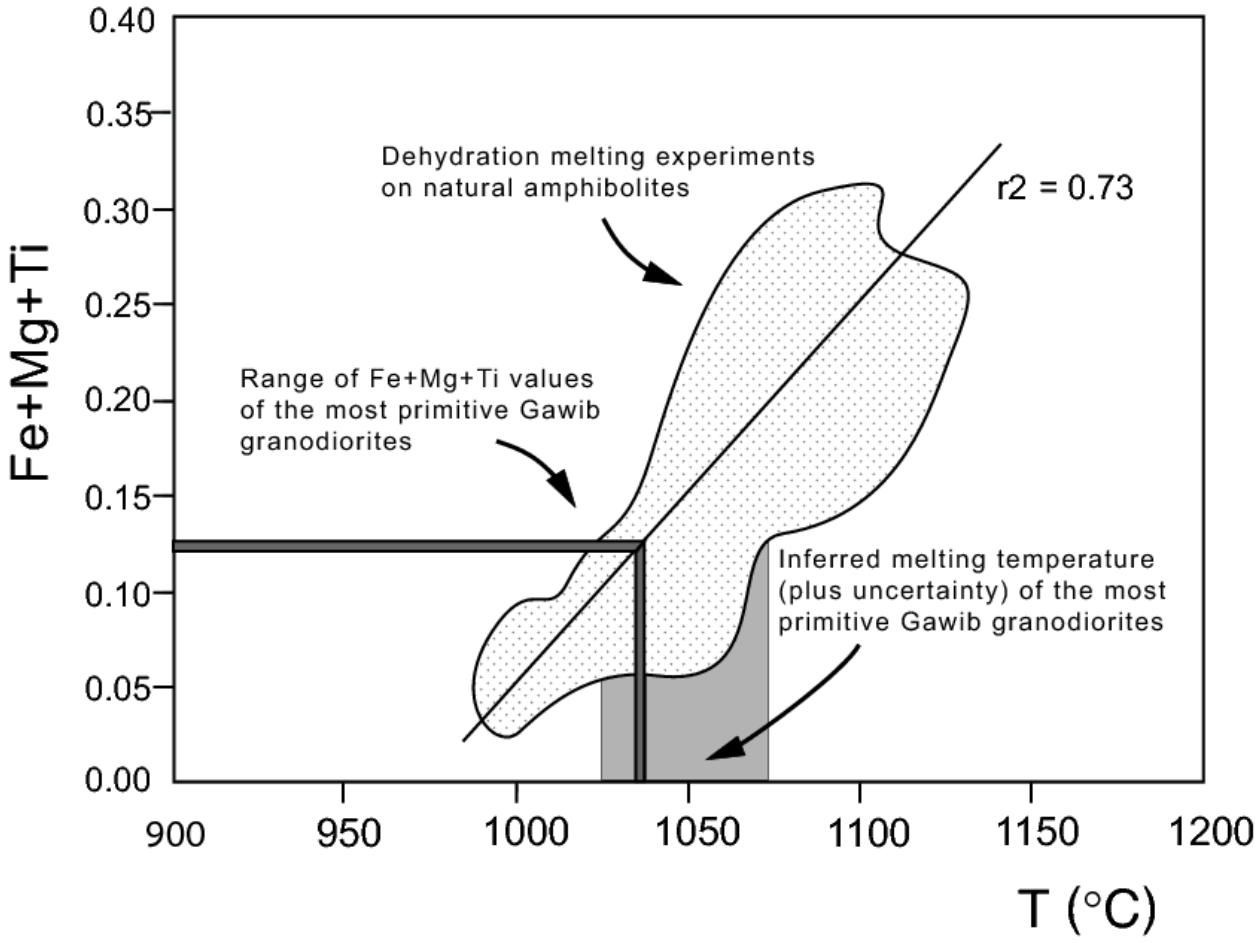

Fig. 15

Table 1. U-Pb zircon data from granodiorite sample M 89 (Gawib pluton, Damara orogen, Namibia)

Analysis no	Isotope ratios:							Ages:					
	$^{206}Pb/^{238}U$	±2σ	$^{207}Pb/^{235}U$	±2σ	$^{207}Pb/^{206}Pb$	±2σ	Rho	$^{206}Pb/^{238}U$	±2σ	$^{207}Pb/^{235}U$	±2σ	$^{207}Pb/^{206}Pb$	±2σ
	Archaean zircon (c. 2.7 Ga)												
Z56	0.542	0.023	14.569	0.686	0.1950	0.004	0.89	2791	95	2788	45	2785	35
	Proterozoic zircon (c. 1.9 Ga), concordant												
Z1	0.345	0.024	5.580	0.420	0.117	0.004	0.91	1912	114	1913	65	1914	56
Z2	0.354	0.017	5.413	0.334	0.111	0.004	0.78	1955	81	1887	53	1813	70
Z15-1	0.351	0.017	5.809	0.306	0.120	0.003	0.90	1939	79	1948	46	1957	42
Z15-2	0.347	0.011	5.754	0.227	0.120	0.003	0.80	1922	52	1940	34	1958	43
Z19	0.350	0.012	5.732	0.234	0.119	0.002	0.87	1932	59	1936	35	1940	36
Z24	0.350	0.011	5.586	0.195	0.116	0.002	0.88	1936	52	1914	30	1890	30
Z64-1	0.349	0.015	5.661	0.254	0.118	0.001	0.96	1930	72	1925	39	1921	21
Z68	0.356	0.015	5.870	0.265	0.120	0.002	0.94	1964	72	1957	39	1949	27
Z78-1	0.358	0.016	6.102	0.300	0.124	0.002	0.94	1972	78	1991	43	2010	31
Z80-1	0.354	0.013	6.193	0.246	0.127	0.002	0.93	1954	62	2003	35	2055	26
Z86	0.362	0.022	6.060	0.382	0.121	0.002	0.97	1991	105	1984	55	1977	28
Z90	0.348	0.021	5.672	0.351	0.118	0.002	0.97	1923	99	1927	53	1932	29
	Proterozoic zircon (c. 1.9 Ga), discordant												
Z11	0.218	0.009	3.269	0.160	0.109	0.003	0.86	1272	49	1474	38	1778	46
Z16	0.229	0.007	3.653	0.121	0.116	0.002	0.90	1328	36	1561	27	1894	26
Z39	0.322	0.007	5.100	0.117	0.115	0.001	0.89	1798	32	1836	20	1880	19
Z40-1	0.311	0.005	4.977	0.081	0.116	0.001	0.90	1746	22	1816	14	1897	13
Z57	0.218	0.010	3.401	0.174	0.113	0.002	0.92	1273	55	1505	40	1848	36
Z69-1	0.178	0.013	2.726	0.210	0.111	0.003	0.96	1055	71	1336	57	1819	41
Z71	0.324	0.013	5.204	0.229	0.116	0.002	0.94	1810	65	1853	38	1902	28
Z81	0.279	0.010	4.620	0.180	0.120	0.002	0.93	1587	51	1753	33	1957	25
Z77	0.275	0.010	4.593	0.190	0.121	0.002	0.92	1567	53	1748	34	1972	28
Z35-1	0.248	0.005	3.726	0.089	0.109	0.001	0.85	1428	26	1577	19	1783	23
	Pan-African zircon (c. 550 Ma), concordant												
Z14-1	0.090	0.003	0.723	0.030	0.059	0.001	0.86	553	19	553	18	549	46
Z22-2	0.089	0.003	0.714	0.025	0.058	0.001	0.88	547	16	547	15	546	36
Z27	0.091	0.003	0.738	0.029	0.059	0.001	0.91	560	19	561	17	565	35
Z32	0.087	0.003	0.709	0.032	0.059	0.002	0.75	541	18	544	19	559	66
Z36	0.090	0.001	0.734	0.013	0.059	0.001	0.79	558	8	559	8	561	24
Z43	0.090	0.003	0.728	0.028	0.058	0.001	0.95	557	20	555	17	548	26
Z48	0.089	0.003	0.727	0.033	0.059	0.002	0.78	551	19	555	20	570	62
Z67	0.089	0.004	0.718	0.032	0.058	0.001	0.90	552	22	549	19	540	43
Z83	0.086	0.003	0.689	0.027	0.058	0.001	0.93	534	18	532	16	523	30
Z84-1	0.087	0.003	0.700	0.029	0.058	0.001	0.92	539	20	539	17	540	35

Z88-2	0.086	0.005	0.691	0.045	0.058	0.002	0.91	534	30	533	27	528	60
Z45-1	0.087	0.003	0.706	0.029	0.059	0.001	0.90	537	19	542	17	565	38
	Pan-African zircon (c. 550 Ma), discordant												
Z4	0.045	0.005	0.342	0.038	0.055	0.002	0.92	282	28	299	28	428	93
Z46-1	0.070	0.003	0.554	0.026	0.058	0.002	0.82	435	16	448	17	517	59
Z50-2	0.073	0.003	0.577	0.023	0.058	0.001	0.90	451	16	463	15	520	38
Z65	0.056	0.003	0.448	0.023	0.058	0.001	0.89	348	15	376	16	548	52
Z70	0.069	0.003	0.569	0.025	0.060	0.001	0.92	431	17	457	16	592	38
Z79-2	0.044	0.002	0.323	0.014	0.054	0.001	0.88	275	10	284	11	356	47

Table 2: Major and trace element composition of country rock gneiss, granodiorites (GD) and granite (G) from the Gawib pluton. LOI: Loss on ignition, n.d.: not determined.

Sample	09/ GW01	09/ GW02	09/ GW05	09/ GW07	02/ GW01	02/ GW02	02/ GW03	M97	M88	M99	M91	M94	M89
Rock type	Gneiss	GD	GD	GD	GD	GD	GD	GD	GD	GD	GD	GD	GD
SiO2	61.05	69.89	65.74	64.97	67.26	65.20	64.53	63.20	63.70	64.59	64.62	65.52	65.67
TiO2	0.96	0.37	0.64	0.55	0.43	0.52	0.67	0.59	0.81	0.46	0.83	0.83	0.68
Al2O3	15.62	15.15	14.97	16.01	14.69	15.24	15.92	15.73	15.09	16.48	14.98	14.27	15.08
Fe2O3	7.17	3.24	5.26	4.48	3.75	4.57	5.91	5.09	6.04	3.74	4.90	5.45	5.20
MnO	0.09	0.09	0.11	0.11	0.08	0.10	0.11	0.12	0.18	0.10	0.15	0.17	0.14
MgO	1.66	0.82	1.71	1.15	1.12	1.42	1.89	1.62	1.65	1.02	1.41	1.49	1.33
CaO	1.85	2.87	3.75	3.75	3.04	3.34	4.10	4.57	4.00	3.69	4.16	3.88	3.65
Na2O	2.88	3.93	3.13	3.83	3.18	3.41	3.15	3.34	3.30	4.00	3.68	3.33	3.29
K2O	7.23	3.28	3.95	3.18	4.69	4.38	4.13	3.06	2.70	3.66	3.07	3.20	2.93
P2O5	0.30	0.17	0.25	0.24	0.17	0.19	0.29	0.32	0.35	0.17	0.32	0.33	0.27
LOI	1.38	0.54	1.00	0.79	1.00	0.92	0.80	0.79	0.63	0.40	0.52	0.65	0.64
SUM	100.2	100.4	100.5	99.06	99.41	99.29	101.5	98.33	98.45	98.31	98.64	99.12	98.88
Ba	2219	736	764	960	720	911	996	914	672	1319	761	886	921
Co	10	4	9	7	6	9	14	13	3	6	4	10	8
Cr	36	8	17	7	2	13	19	n.d.	10	3	4	11	11
Cu	0	13	8	10	n.d.	n.d.	n.d.	n.d.	n.d.	n.d.	n.d.	n.d.	n.d.
Ga	16	13	14	17	20	22	19	21	21	21	21	18	19
Nb	20	16	23	28	21	26	27	15	37	20	40	38	32
Ni	13		6	5			17		20	17	12	16	16
Pb	37	23	28	22	24	28	28	15	20	43	23	31	24
Rb	313	140	173	144	192	198	212	125	113	121	124	137	107
Sc	17	4	18	9	2	7	14	9	10	3	15	11	9
Sr	151	671	560	734	631	756	642	693	716	939	748	713	741
Th	19	18.9	24.7	18.0	34.7	25.4	27.4	14	31	24	39	30	25
U	30.2	4.3	4.9	4.5	8.1	6.0	4.6	4.6	3	3	4	4	7

V	77	35	82	58	24	24	29	26	46	28	47	46	39
Y	29	21	30	33	57	75	86	65	50	50	63	70	47
Zn	88	49	59	59	50	58	72	70	110	67	86	93	87
Zr	360	170	234	219	190	222	298	190	320	197	332	328	288
Hf	n.d.	4.4	6.4	5.5	4.8	5.7	7.4	n.d.	n.d.	n.d.	n.d.	n.d.	n.d.
Ta	n.d.	1.4	2.0	2.5	1.8	1.8	2.1	n.d.	n.d.	n.d.	n.d.	n.d.	n.d.
La	73.7	43.1	62.1	57.1	48.8	57.8	76.1	50.3	95.4	56.6	94	64	75.1
Ce	149	81.3	120	111	94	110	139	98.1	178	106	197	126	143
Pr	16.1	8.66	12.9	12.5	10.0	11.7	14.3	n.d.	n.d.	n.d.	n.d.	n.d.	n.d.
Nd	58.6	31.2	46.3	45.7	35.2	41.3	49.8	42.4	65.9	38.1	67.9	45.4	52.9
Sm	10.3	5.50	8.50	8.90	6.20	7.10	8.20	8.53	13.4	8.48	14.4	9.87	10.8
Eu	1.50	1.30	1.68	1.99	1.26	1.42	1.69	1.66	3.06	1.62	2.63	1.66	2.49
Gd	7.80	4.20	6.30	7.10	4.50	5.30	6.10	5.68	9.9	5.15	9.59	7.12	8.33
Tb	1.1	0.6	0.9	1.0	0.6	0.7	0.8	n.d.	n.d.	n.d.	n.d.	n.d.	n.d.
Dy	5.9	3.3	5.1	5.6	3.6	3.9	4.4	4.42	7.14	3.50	6.68	5.52	6.8
Ho	1.1	0.6	1.0	1.0	0.7	0.7	0.8	n.d.	n.d.	n.d.	n.d.	n.d.	n.d.
Er	3.1	1.9	2.8	3.1	2.0	2.1	2.3	2.0	3.8	1.7	4.1	3.3	3.8
Tm	0.46	0.28	0.42	0.47	0.3	0.32	0.34	n.d.	n.d.	n.d.	n.d.	n.d.	n.d.
Yb	3.0	1.9	2.8	3.2	2.0	2.1	2.2	1.5	3.2	1.5	3.0	2.8	2.9
Lu	0.51	0.32	0.45	0.52	0.35	0.36	0.35	0.22	0.54	0.24	0.46	0.40	0.42

Table 2. (cont.)

Sample	M87	M98	M95	M90	M96	M92	M93	09/ GW03	09/ GW04	09/ GW06	02/ GW04
Rock type	GD	GD	GD	GD	GD	G	G	G	G	G	G
SiO2	65.69	66.80	66.83	67.29	67.77	74.15	74.62	72.54	76.07	74.25	70.73
TiO2	0.48	0.34	0.60	0.41	0.37	0.05	0.07	0.14	0.08	0.09	0.24
Al2O3	16.47	15.95	13.93	15.65	14.98	13.76	13.49	14.33	12.87	13.82	14.46

Fe2O3	3.87	3.08	5.26	3.33	3.08	0.60	0.79	1.21	0.89	1.00	1.69
MnO	0.10	0.11	0.14	0.09	0.09	0.02	0.02	0.03	0.02	0.03	0.05
MgO	1.06	0.99	1.33	0.93	0.81	0.08	0.11	0.40	0.15	0.19	0.61
CaO	3.56	3.28	3.56	3.38	3.21	0.98	1.13	1.75	0.74	1.55	2.06
Na2O	3.96	3.53	3.33	3.81	4.06	2.98	3.36	3.46	2.99	3.28	3.56
K2O	3.49	3.83	2.83	3.32	2.74	5.69	4.81	4.90	5.86	5.19	4.08
P2O5	0.18	0.13	0.24	0.17	0.14	0.04	0.02	0.06	0.03	0.04	0.10
LOI	0.64	1.12	0.19	0.53	0.78	0.78	0.95	1.09	0.74	0.71	0.66
SUM	99.50	99.16	98.24	98.91	98.03	99.13	99.37	99.91	100.4	100.2	98.24
Ba	1207	1080	732	1093	601	146	327	914	359	617	1108
Co	3	6	5	3	3	6	1	1	1	2	3
Cr	n.d.	3	9	1	n.d.	3	3	7	5	4	3
Cu	n.d.	n.d.	n.d.	n.d.	n.d.	n.d.	n.d.	4	2	11	n.d.
Ga	20	18	19	22	14	14	11	14	13	12	14
Nb	22	24	26	18	16	10	9	9	11	8	9
Ni		16	3	18				2	2	2	20
Pb	21	33	23	20	26	71	57	28	19	37	51
Rb	123	176	118	120	122	281	225	157	177	175	178
Sc	3	6	12	8	4	8	2	4	4	10	9
Sr	902	818	714	853	697	84	200	453	259	332	523
Th	12	26	22	16	16	15	17	6.0	19.0	13.5	8.2
U	3	6	4	8	4	7	9	2.1	4.0	3.6	2.5
V	24	25	35	24	21	27	16	19	21	10	15
Y	35	24	58	28	34	11	7	10	8	6	15
Zn	67	126	86	65	59	7	3	10	7	13	29
Zr	206	170	244	178	167	45	50	75	44	59	93
Hf	n.d.	n.d.	n.d.	n.d.	n.d.	n.d.	n.d.	2.2	2.4	2.0	2.4
Ta	n.d.	n.d.	n.d.	n.d.	n.d.	n.d.	n.d.	0.6	1.0	0.5	0.5
La	57.6	53.8	70	49.1	41.6	29.5	n.d.	22.2	9.9	11.3	21.4
Ce	109	98.8	130	83.5	77.5	69.8	n.d.	40.7	16.8	20.9	39.1
Pr	n.d.	n.d.	n.d.	n.d.	n.d.	n.d.	n.d.	4.24	1.65	2.17	4.08
Nd	39.0	35.0	48.2	33.3	26.3	30.8	n.d.	14.8	5.60	7.70	14.4
Sm	7.94	7.24	10.5	7.1	6.04	6.66	n.d.	2.6	1.00	1.40	2.50
Eu	1.7	1.42	2.29	1.43	1.29	1.13	n.d.	0.75	0.28	0.50	0.95

Gd	6.04	4.94	7.71	4.39	4.56	4.92	n.d.	1.9	0.80	1.10	1.80
Tb	n.d.	n.d.	n.d.	n.d.	n.d.	n.d.	n.d.	0.3	0.13	0.16	0.20
Dy	4.00	4.10	5.25	4.26	3.73	4.24	n.d.	1.5	0.80	0.90	1.20
Ho	n.d.	n.d.	n.d.	n.d.	n.d.	n.d.	n.d.	0.3	0.18	0.20	0.25
Er	2.0	2.1	2.9	2.3	2.0	2.0	n.d.	0.8	0.50	0.60	0.70
Tm	n.d.	n.d.	n.d.	n.d.	n.d.	n.d.	n.d.	0.12	0.09	0.10	0.10
Yb	1.7	2.2	2.3	1.6	1.6	1.7	n.d.	0.8	0.80	0.80	0.70
Lu	0.26	0.34	0.40	0.20	0.25	0.24	n.d.	0.15	0.16	0.16	0.13

Table 3. Rb-Sr. Sm-Nd whole rock data and Pb-isotope ratios obtained on acid-leached K-feldspar from granodiorites and granites from the Gawib pluton.
Analytical methods are described in Appendix A. 87Rb/86Sr and 147Sm/144Nd are calculated from ICP-MS data. Calculation of εNd values is relative to CHUR
according to Jacobsen and Wasserburg (1980). Nd model age (TDM) calculation is according to Michard et al. (1985). (m): measured.
(i): initial

		$^{87}Sr/^{86}Sr(m)$	error	$^{87}Rb/^{86}Sr$	$^{87}Sr/^{86}Sr(i.)$	$^{143}Nd/^{144}Nd(m.)$	error	$^{147}Sm/^{144}Nd$	$^{143}Nd/^{144}Nd(i.)$	ε Nd (i)	T(DM)	$^{206}Pb/^{204}Pb$	$^{207}Pb/^{204}Pb$	$^{208}Pb/^{204}Pb$
09/GW01	Gneiss	0.822527	0.000003	6.00	0.775483	0.511200	0.000003	0.106	0.510817	-21.7	2.5	n.d.	n.d.	n.d.
09/GW02	GD	0.717917	0.000003	0.60	0.713182	0.511757	0.000002	0.107	0.511373	-10.9	1.8	n.d.	n.d.	n.d.
09/GW05	GD	0.717209	0.000003	0.89	0.710198	0.511858	0.000003	0.111	0.511458	-9.2	1.7	n.d.	n.d.	n.d.
09/GW07	GD	0.716636	0.000003	0.57	0.712183	0.511847	0.000002	0.118	0.511423	-9.9	1.8	n.d.	n.d.	n.d.
02/GW01	GD	0.715127	0.000007	0.88	0.708556	0.511928	0.000012	0.106	0.511544	-7.5	1.6	n.d.	n.d.	n.d.
02/GW02	GD	0.713956	0.000008	0.76	0.708300	0.511930	0.000012	0.104	0.511555	-7.3	1.5	17.89	15.60	38.51
02/GW03	GD	0.716930	0.000008	0.96	0.709799	0.511871	0.000012	0.100	0.511512	-8.1	1.5	17.69	15.61	38.35
M97	GD	0.715252	0.000008	0.52	0.711357	0.511749	0.000012	0.122	0.511311	-12.1	2.1	17.71	15.58	38.12
M88	GD	0.715915	0.000006	0.46	0.712507	0.511808	0.000012	0.123	0.511365	-11.0	2.0	n.d.	n.d.	n.d.
M99	GD	0.715183	0.000008	0.37	0.712309	0.511814	0.000012	0.135	0.511329	-11.7	2.3	17.63	15.59	38.20
M91	GD	0.716351	0.000009	0.48	0.712673	0.511814	0.000012	0.128	0.511352	-11.3	2.1	n.d.	n.d.	n.d.
M94	GD	0.717029	0.000007	0.56	0.712803	0.511797	0.000012	0.131	0.511323	-11.8	2.2	17.48	15.61	38.24
M89	GD	0.715932	0.000008	0.42	0.712771	0.511821	0.000012	0.123	0.511376	-10.8	2.0	17.45	15.56	38.07
M87	GD	0.715576	0.000003	0.39	0.712481	0.511793	0.000012	0.123	0.511349	-11.3	2.0	17.53	15.58	38.14
M98	GD	0.714589	0.000003	0.62	0.709706	0.511906	0.000012	0.125	0.511455	-9.3	1.9	n.d.	n.d.	n.d.
M95	GD	0.716368	0.000009	0.48	0.712644	0.511816	0.000012	0.132	0.511341	-11.5	2.2	n.d.	n.d.	n.d.
M90	GD	0.715846	0.000003	0.41	0.712653	0.511765	0.000012	0.129	0.511300	-12.3	2.2	n.d.	n.d.	n.d.
M96	GD	0.717426	0.000003	0.51	0.713453	0.511752	0.000012	0.139	0.511252	-13.2	2.5	n.d.	n.d.	n.d.
M92	G	0.801664	0.000009	9.68	0.725742	0.511596	0.000012	0.106	0.511214	-14.0	2.0	17.56	15.55	38.00
M93	G	0.744749	0.000003	3.26	0.719216	0.511602	0.000012	0.106	0.511220	-13.9	2.0	n.d.	n.d.	n.d.
09/GW03	G	0.727221	0.000003	1.00	0.719355	0.511401	0.000002	0.106	0.511018	-17.8	2.2	n.d.	n.d.	n.d.
09/GW04	G	0.727841	0.000003	1.98	0.712331	0.511626	0.000002	0.108	0.511237	-13.5	2.0	17.49	15.63	38.12

09/GW06	G	0.728585	0.000002	1.53	0.716622	0.511569	0.000003	0.110	0.511173	-14.8	2.1	17.92	15.68	38.71
02/GW04	G	0.728883	0.000008	0.99	0.721533	0.511438	0.000012	0.105	0.511060	-17.0	2.2	17.82	15.65	38.38

Highlights

Geochemical data from high-T granodiorites and granites imply lower crustal amphibolite melting.

New U-Pb zircon ages imply syn-orogenic intrusion

New Sr-Nd-Pb isotope data imply ancient crustal sources and constrain AFC processes